UNIVERSIDADE FEDERAL DA BAHIA
INSTITUTO DE GEOCIÊNCIAS
CURSO DE OCEANOGRAFIA

MIRELA GOIS BATISTA

UM ESTUDO PRELIMINAR DA SENSIBILIDADE DO MODELO OCEÂNICO HYCOM A PERTURBAÇÕES NA CONDIÇÃO INICIAL E NA FORÇANTE ATMOSFÉRICA AO LARGO DA COSTA SUDESTE DO BRASIL

Salvador
2017

MIRELA GOIS BATISTA

UM ESTUDO PRELIMINAR DA SENSIBILIDADE DO MODELO OCEÂNICO HYCOM A PERTURBAÇÕES NA CONDIÇÃO INICIAL E NA FORÇANTE ATMOSFÉRICA AO LARGO DA COSTA SUDESTE DO BRASIL

Monografia apresentada ao curso de graduação em Oceanografia, Instituto de Geociências, Universidade Federal da Bahia, como requisito parcial para a obtenção do grau de bacharel em Oceanografia. Este trabalho é apresentado na forma de um manuscrito que será submetido para a Revista Brasileira de Oceanografia.

Orientador: Prof. Dr. Clemente Augusto Souza Tanajura

Salvador
2017

TERMO DE APROVAÇÃO

MIRELA GOIS BATISTA

ESTUDO PRELIMINAR DA SENSIBILIDADE DO MODELO OCEÂNICO HYCOM A PERTURBAÇÕES NA CONDIÇÃO INICIAL E NA FORÇANTE ATMOSFÉRICA AO LARGO DA COSTA SUDESTE DO BRASIL

Monografia aprovada como requisito parcial para a obtenção do grau de bacharel em Oceanografia, pela seguinte banca examinadora:

Clemente Augusto Souza Tanajura
Ph.D. em Meteorologia - Departamento de Meteorologia da Universidade de Maryland, EUA.
Universidade Federal da Bahia (UFBA), Brasil.

Carlos Alessandre Domingos Lentini
Ph.D. em Meteorologia e Oceanografia – Escola Rosenstiel de Ciências Marinha e Atmosférica, Universidade de Miami, EUA.
Universidade Federal da Bahia (UFBA), Brasil.

Janini Pereira
Doutora em Oceanografia (Oceanografia física) - Universidade de São Paulo (USP), Brasil.
Universidade Federal da Bahia (UFBA), Brasil.

Salvador, 04 de setembro de 2017

APRESENTAÇÃO

Este trabalho é apresentado na forma de um manuscrito em inglês que será submetido para a Revista Brasileira de Oceanografia.

“I feel the weight of the world on my shoulder
As I'm getting older, y'all, people gets colder
Most of us only care about money making
Selfishness got us followin' in the wrong direction

Wrong information always shown by the media.
Negative images is the main criteria
Infecting the young minds faster than bacteria
Kids wanna act like what they see in the cinema
Yo', whatever happened to the values of humanity
Whatever happened to the fairness in equality
Instead of spreading love we’re spreading animosity
Lack of understanding, leading lives away from unity

That's the reason why sometimes I'm feeling under
That's the reason why sometimes I'm feeling down
There's no wonder why sometimes I'm feeling under
Gotta keep my faith alive ‘til love is found

Father, Father, Father help us
send some guidance from above
'Cause people got me, got me questionin'
Where is the love?”
Black Eyed Peas – Where is the love

AGRADECIMENTOS

Sou extremamente grata a todos os ventos e mares que me guiaram até aqui e a todas as forças do universo que me trouxeram até este último degrau da graduação.

Gostaria de agradecer primeiramente aos meus pais, Clésia e Bernardo, por todo o incentivo material e imaterial que me deram durante esses seis anos dentro da UFBA. Não sei o que teria sido de mim sem a imensa ajuda e todo o suporte de vocês. Muito obrigada, amo vocês! Gostaria de agradecer ao meu irmão, Ciro, e à minha cunhada, Fernanda, além de toda a minha família, principalmente meus avós, que são meus exemplos. Eu os amo muito e tenho muito orgulho de vocês. Um agradecimento especial a Tobias, meu gato de estimação, que esteve comigo nesses últimos quatro anos da graduação e só precisava chegar perto de mim e ficar ao meu lado para me transmitir boas energias e acabar com qualquer estresse meu.

Um imenso obrigada à professora Janini por ser uma inspiração feminina dentro da oceanografia física para mim e por ter proporcionado o meu primeiro contato com o Matlab, acreditando em mim. Agradeço também ao meu orientador Clemente por todo o suporte e orientação neste último ano de graduação. Todos os ensinamentos passados até aqui foram fundamentais para quem eu sou hoje dentro da oceanografia física. Agradeço novamente à professora Janini Pereira e também a Carlos Lentini, que compõem a banca examinadora, pelas contribuições dedicadas a este trabalho. E agradeço também ao professor Mauro Cirano, por ter sido o primeiro a me inspirar e despertar o meu interesse pela oceanografia física.

Agradeço a todos os meus amigos da faculdade, que tornaram os meus dias dentro deste ambiente muito mais fáceis e leves. Em especial para a minha turma de 2011. Aos colegas do laboratório, que ouviram todas as minhas dificuldades e desespero dentro desse último ano, e me proporcionaram boas risadas e bons momentos dentro da Sala 19. Vocês todos foram muito especiais neste trabalho, obrigada por todo o suporte. Em especial a Rodrigo, Leonardo, Nanda Matos, Julia e Ingrid, que não devem mais aguentar me ouvir falar de TCC dentro e fora do laboratório!

Não posso deixar de agradecer a Filipe Costa. Se não fosse por ele eu não teria aprendido nem 10% de tudo o que eu sei hoje sobre Linux e Matlab. Você foi essencial para o meu crescimento profissional com este trabalho, e eu vou ser eternamente grata por isto. Obrigada também a todos os outros que me ajudaram direta ou indiretamente neste trabalho: Rafael, Vitor, Carlos e José Roberto. Vocês sempre me acudiram sempre que precisei, estando sempre dispostos a ajudar. Obrigada por todo o suporte!

Obrigada a toda a equipe da REMO, pela oportunidade e pelos dados oferecidos, e de Física Nuclear, por todo o acolhimento dentro do ambiente de trabalho.

Gostaria de agradecer especialmente à família Barrouin Oliveira que me incentivou imensamente a ir para o intercâmbio. A ajuda, conselho e apoio de vocês foi fundamental em minha vida. Serei eternamente grata!

Obrigada a Beatriz Cedraz por sempre ter estado presente em todas as situações difíceis, sempre me apoiando. À Tallitha Mercês por toda a aproximação ao longo desses últimos anos e por sempre me animar e me colocar para cima. E um obrigada especial a Daniel Almeida por ter estado ao meu lado, me proporcionando muitos momentos felizes e me ajudando a manter a calma, enquanto eu desabafava sobre a monografia.

Obrigada também ao CNPq e ao PIBIC/UFBA pelo apoio financeiro a este projeto de pesquisa. Agradeço também ao programa Ciência sem Fronteiras que junto à CAPES contribuiu financeiramente para a melhor experiência da minha vida, o intercâmbio na Noruega. Conheci mais um monte de pessoas incríveis, as quais também gostaria de agradecer. Obrigada Alisa, Misha, Rina, Amanda, Mélanie, Merve, Bernie, Lasse, Barbie, Aleksander, e todos os outros amigos de Bodø e Svalbard pelas experiências incríveis e por terem me acolhido de forma tão carinhosa e confortável, que me senti em casa mesmo bem longe dela.

Obrigada a todos! Sem vocês eu **não** teria chegado até aqui!

RESUMO

A realização de um conjunto de previsões é uma estratégia importante para melhorar a previsibilidade de modelos oceânicos e abrir a possibilidade de empregar métodos de assimilação de dados baseados em conjuntos. No presente trabalho, a sensibilidade do modelo *Hybrid Coordinate Ocean Model* (HYCOM) a perturbações na condição inicial e forçante atmosférica foi avaliada como um passo preliminar para a construção de um *Ensemble Kalman Filter* (EnKF) no escopo da Rede de Modelagem e Observação Oceanográfica (REMO). Um estudo de previsibilidade curta a estendida foi realizado com ênfase em um vórtice ciclônico ao largo do Sudeste do Brasil. O HYCOM foi configurado com 1/12° de resolução horizontal e 21 camadas verticais na região 65°W-20°W/55°S-10°N. Quarenta e três membros construídos a partir de 4 estratégias diferentes formaram um conjunto de previsões em uma janela de 30 dias inicializada em 16 de abril de 2011. As estratégias consistiram em: (i) considerar diferentes magnitudes relativas dos incrementos de análise; (ii) aumentar ou reduzir as entradas da matriz de covariância de erro das observações; (iii) adicionar ou subtrair o desvio padrão da temperatura e dos componentes horizontais da velocidade; (iv) perturbar a velocidade do vento e fluxos de momentum com anomalias derivadas das saídas da forçante atmosférica. O impacto de cada estratégia foi avaliado através do cálculo do desvio padrão da temperatura e da anomalia do nível do mar. Os resultados mostraram uma maior contribuição da estratégia 4 na geração do espalhamento, seguida da estratégia 2, estratégia 1 e estratégia 3. Analisando o conjunto, na temperatura da superfície do mar houve um aumento de aproximadamente 27,7% no desvio padrão, seguido de 47,1% e 61,5% em 50 m e 100 m, respectivamente. O aumento do desvio padrão médio da anomalia do nível do mar foi de cerca de 42,8% ao longo do tempo de integração de 30 dias. As perturbações da forçante atmosférica aumentaram o espalhamento do conjunto ao longo dos 30 dias para a área de estudo. As trilhas percorridas pelo vórtice podem diferir de acordo com cada membro do conjunto, especialmente no dia 30. Porém, o conjunto manteve o sinal do vórtice na superfície, mas exibiu diferentes formatos e posições para o vórtice. A fonte de erro imposta à forçante atmosférica produziu a principal contribuição para o espalhamento e covariância do conjunto em todo o espaço tridimensional. Para este evento específico localizado no sudeste do Brasil, o EnKF deve ser iniciado com perturbações na forçante atmosférica.

Palavras-chave: Previsão por conjuntos; HYCOM; EnOI; Assimilação de dados; Corrente do Brasil

ABSTRACT

Ensemble forecast is an important strategy to improve ocean model short-range to extended predictability and to open the possibility to employ ensemble-based data assimilation methods. In the present work, the Hybrid Coordinate Ocean Model (HYCOM) sensitivity to perturbations in the initial condition and atmospheric forcing was assessed as a preliminary step toward the construction of an Ensemble Kalman Filter (EnKF) under the Brazilian Oceanographic Modelling and Observation Network (REMO). The short to extended predictability study focused on forecasting a specific cyclonic eddy in Southeast Brazil. HYCOM was configured with 1/12° of horizontal resolution and 21 vertical layers over the region 65°W-20°W/55°S-10°N. Forty-three ensemble members were employed to produce 30-day forecasts initialized on 16 April 2011. Four different strategies were used by: (i) considering different relative magnitudes of the analysis increments; (ii increasing or reducing the entries of the observation error covariance matrix; (iii) adding or subtracting the standard deviation of the temperature and horizontal components of the velocity; (iv) perturbing the wind stress and momentum fluxes with anomalies derived from atmospheric forcing outputs. The impact of each strategy was evaluated by calculating the temperature and sea level anomaly standard deviation. Results showed greater contribution of the strategy 4 on generating spreading, followed by strategy 2, strategy 1 and strategy 3. Analysing the ensemble, at the surface, there was an increase of approximately 27.7% in the mean temperature standard deviation, followed by 47.1% and 61.5% at 50 m and 100 m, respectively. The increase in the mean sea level anomaly standard deviation was about 42.8% throughout the 30-day integration time. Perturbations in the atmospheric forcing increased the ensemble spread in the lead-time of 30 days for the study area. By analysing the eddy behaviour, its tracks may differ according to each member, especially on the day 30. However, the ensemble kept the eddy signal at the surface, but showed different eddy shapes and positions. The error source imposed on the atmospheric forcing produced the main contribution to the ensemble spread and covariance in the entire three-dimensional space. To this specific event located in southeast of Brazil the EnKF should be started with perturbations in the atmospheric forcing.

Keywords: Ensemble forecast; HYCOM; EnOI; Data assimilation; Brazil Current.

LIST OF FIGURES

LIST OF TABLES

LIST OF ACRONYMS

AAIW	Antarctic Intermediate Water
ADCP	Acoustic Doppler Current Profiler
AMRS-E	Advanced Microwave Scanning Radiometer – Earth Observing System
AVISO	Archiving, Validation and Interpretation of Satellite Oceanographic Data
BC	Brazil Current
CENPES	Leopoldo Américo Miguez de Mello Research Centre of PETROBRAS
CERSAT	Centre ERS d'Archivage et de Traitement
CFS	Climate Forecasting System version 2
CFSR	Climate Forecasting System Reanalysis
CHM	Hydrography and Navigation Centre of the Brazilian Navy
COADS	Comprehensive Ocean Atmosphere Data Set
CST	Cape São Tomé
CTD	Conductivity, temperature and density
EnKF	Ensemble Kalman Filter
EnOI	Ensemble Optimal Interpolation
ETOPO2	Earth Topography 2
FAG	Faghmous et al., 2015
GHRSST	Group for High Resolution Sea Surface Temperature
GODAE	Global Ocean Data Assimilation Experiment
HYCOM	HYbrid Coordinate Ocean Model
IWBC	Intermediate Western Boundary Current
MIC	Members with perturbed initial condition
MICOM	Miami Isopycnic Coordinate Ocean Model
MFORC	Members with perturbed atmospheric forcing
MOVAR	Monitoring the upper Ocean transport variability in the western South Atlantic
NCAR	National Center for Atmospheric Research
NCEP	National Centers for Environmental Prediciton
NERSC	Nansen Environmental and Remote Sensing Centre
NOAA	National Oceanic and Atmospheric Administration
OFS	Ocean Forecasting Systems

OSTIA	Operational Sea Surface Temperature and Sea Ice Analysis
REMO	Brazilian Oceanographic Modelling and Observation Network
RODAS	REMO Ocean Data Assimilation System
S	Salinity
SACW	South Atlantic Central Water
SD	Standard Deviation
SLA	Sea Level Anomaly
SSH	Sea Surface Height
SST	Sea Surface Temperature
T	Temperature
TOPAZ	(Towards) an Operational Prediction system for the North Atlantic European Zones
TW	Tropical Water
U	Zonal Component of the velocity
UBFA	Federal University of Bahia
UFLX	Zonal component of the momentum flux
UFRJ	Federal University of Rio de Janeiro
UGRD	Zonal component of the wind 10 m above the ground
V	Meridional component of the velocity
VFLX	Meridional component of the momentum flux
VGRD	Meridional component of the wind 10 m above the ground
WOA	World Ocean Atlas
XBT	EXpendable BathyThermography

LIST OF SYMBOLS

x^a	Analysis
x^f	First guess/prior state/model background state
Y	Vector of observations
H	Linear observation operator matrix
$Y-\mathcal{H}X^b$	Innovation vector
$K(Y-\mathcal{H}X^b)$	Analysis increment
K	Kalman gain matrix
B	Background error covariance matrix
R	Diagonal covariance matrix of the observational error
α	Scalar to restrain the magnitude of the analysis increment
σ	Localization operator
o	Schur product
A	Anomalies

TABLE OF CONTENTS

1 Introduction

Ocean forecasting systems (OFS) are necessary for a variety of activities: oil and gas exploitation; maritime safety for navigation; studies of climate change; coastal management and pollution dispersion; search and rescue operations; fishing, among others (Schiller et al., 2015). OFS predict the state of currents, sea temperature and salinity, the distribution of the mixed layer depth, current meandering and eddies in the three-dimensional field (Hurlburt et al., 2009, Srinivasan et al., 2011). OFS must be capable of providing high-quality nowcasts and forecasts of the ocean state. These products become feasible nowadays with the availability of real-time data, accurate numerical models, ocean data assimilation systems and sufficient computing power (Hurlburt et al., 2008). The OFS ability to hand over high-quality products partially relies on efficient data assimilation schemes. They statistically combine key observations from satellites and from in situ data with high-resolution ocean model outputs, providing improved initial conditions and more accurate representation of the ocean state and circulation (Bell et al., 2015).

Data assimilation systems use information of observational data combined with short-range model forecasts (background) to provide the analysis, aiming to correct the model state toward the observational data (Talagrand 1997; Kalnay 2003). Taking into consideration that satellites only measure quantities of the ocean surface and in situ data are sparse, numerical ocean models are fundamental to extrapolate information of observed data in space and time, carrying information from data-rich to data-poor areas (Kalnay 2003; Zaron 2011). An eddy-resolving model like the Hybrid Coordinate Ocean Model (HYCOM) is a suitable tool to depict oceanic mesoscale features, and to be employed in conjunction with data assimilation systems (Hurlburt et al., 2009).

The ocean mesoscale eddies are dynamically similar to the ones in the atmosphere. However, oceanic eddies have length-scales in the order of dozens of kilometres, whilst the atmospheric eddies may have greater dimensions. This fundamental difference requires an eddy-resolving ocean model to have higher horizontal resolution and attains large computational cost over basin scale domains (Bryan 2008; Sakov et al., 2012).

Using twin-forecasts, but one with a small perturbation added in the initial condition, Lorenz (1963, 1965) discovered that even with perfect initial conditions, a numerical model has a limit of predictability. Over time, the previous forecast and the perturbed one showed spreading in the states of the atmosphere due to its chaotic nature. Therefore, stochastic forecasts would provide better estimates of the real state of the atmospheric or oceanic flows. Computationally, it is achievable through ensemble forecasting - several different stochastic model forecasts, with perturbations introduced in the initial condition or observations.

Data assimilation and ensemble forecasting are connected by the fact that ensembles estimate the model uncertainty of the forecast-flow and data assimilation methods claim to produce the best evaluation of the short-term forecast error (Hamill 2006). Therefore, ensemble-based assimilation systems use a finite number of forecasts to compute the analysis uncertainty in the assimilation process. Ensemble forecasting yields a more accurate forecast by averaging all the ensemble members (Kalnay 2003). This is an advantage of stochastic forecasts over deterministic forecasts, which only display one possible path that can possibly diverge from the truth.

A good quality ensemble envelops the observation (considered as the true state) and the ensemble mean is closer to observation than a member randomly chosen. A bad ensemble would collapse with time, showing a small dispersion, and do not envelope the true state. Through ensemble forecasting, the predictive ability of the numerical model is known, by analysing the ensemble spreading that perturbed initial conditions or atmospheric forcing may result. The average of these stochastic forecasts would be the best product the model could offer (Leith 1974).

A widely used ensemble forecasting technique is the Ensemble Optimal Interpolation (EnOI), which is a simplification of the Ensemble Kalman Filter (EnKF), introduced by Evensen (1994) and Burgers et al. (1998). EnOI (Evensen 2003) requires stationary ensemble members from a long model run to estimate the model error covariance matrix that will not be altered throughout time. Although the ensemble is static in time, the ensemble members in EnOI greatly describe the spatial correlations and the oceanic circulation, keeping the analysis dynamically consistent. The stationary ensemble greatly reduces the computational cost, which makes the EnOI very favourable for operational applications, despite providing a suboptimal

solution when compared to EnKF (Oke et al., 2007) and do not give coherent error estimates for the analysis. Another approach to produce an estimate of the model error covariance matrix with the EnOI is to select different ensemble members depending on the assimilation day or season, as it was done in Xie and Zhu (2010), Tanajura et al. (2014) and Mignac et al. (2015). This approach is particularly important in regions with strong seasonal cycle.

The EnKF, contrastingly, uses an ensemble step forward integration in which the time-dependent model error statistics is calculated from a stochastically perturbed ensemble (Melsom et al., 2012). This method tries to capture the so-called “error of the day”, i.e. the specific model error patterns on the assimilation day. The EnKF requires *n* model integrations to represent the model error covariance in the next assimilation step, which means an increase of the computational cost by *n* (Oke et al., 2010). Nevertheless, the spreading performed by a perturbed ensemble greatly shows the forecast error (Melsom et al., 2012), while EnOI neither represent the daily uncertainties of the model nor the forecast errors, since it does not have a time-forward ensemble forecasting (Oke et al., 2010).

Houtekamer and Zhang (2016) proposed a recent review for the utilization of the EnKF in the atmospheric data assimilation. In the ocean, the only operational data assimilation system that employs the EnKF is the TOPAZ - (Towards) an Operational Prediction system for the North Atlantic European Coastal Zones (Sakov et al., 2012). TOPAZ employs an ocean-sea ice coupled system for the North Atlantic and Arctic Ocean, using HYCOM coupled to a one-thickness category sea ice model. The Nansen Environmental and Remote Sensing Centre (NERSC/Norway) developed TOPAZ (http://topaz.nersc.no/). TOPAZ assimilates 1) along-track sea level anomalies (SLA) from Jason family satellites; 2) sea surface temperature (SST) from the Operational Sea Surface Temperature and Sea Ice Analysis (OSTIA); 3) sea ice drift data from the *Centre ERS d’Archivage et de Traitement* (CERSAT); 4) ice concentration by the Advanced Microwave Scanning Radiometer - Earth Observing System (AMSR-E). The assimilation occurs at every seven days (Sakov et al., 2012).

In Brazil, the Oceanographic Modelling and Observation Network (REMO) (www.rederemo.org) developed the REMO ocean data assimilation system (RODAS) into HYCOM as a new element of an operational ocean forecasting system for the

Atlantic Ocean (Lima et al., 2013, Tanajura et al., 2014, Mignac et al., 2015). REMO is a research group currently composed of researchers from the Federal University of Bahia (UFBA), the Federal University of Rio de Janeiro (UFRJ), the Hydrography and Navigation Centre of the Brazilian Navy (CHM) and the Leopoldo Américo Miguez de Mello Research Centre of PETROBRAS (CENPES). RODAS was developed under international collaboration with the HYCOM Consortium, the Global Ocean Data Assimilation Experiment (GODAE) Ocean View project (Chassignet et al., 2009; Dombrowsky et al., 2009) and the Institute of Atmospheric Physics by the Chinese Academy of Sciences. Developed at UFBA, HYCOM+RODAS represents a joint effort of all the groups involved in REMO. RODAS is based on the Ensemble Optimal Interpolation scheme (Tanajura et al., 2014), using the algorithms suggested in Xie and Zhu (2010), Yan et al. (2010), and Xie et al. (2011). RODAS assimilates sea surface temperature data, gridded or along-track sea level anomaly data from altimeters, and vertical profiles of temperature and salinity (T/S) (Tanajura et al., 2014; Costa and Tanajura 2015; Mignac et al., 2015). REMO aims the scientific and technological development in physical oceanography, employing operational ocean forecast systems and ocean modelling with assimilation of high quality data for the Metarea V area (between 36° S and 7° N and from 20° W to the coast of Brazil). This region is under responsibility of the Brazilian Navy in accordance with the commitments made as part of the International Convention for the Safety of Life at Sea.

The Metarea V, more specifically the southeast coast of Brazil, holds intense mesoscale activity developed by the Brazil Current (BC). The mesoscale variability in the ocean is characterized by transient features like eddies, meanders and waves. Eddies are frequent features in the ocean defined by quasi-circular or elliptical shapes, with closed contours of sea surface height (Lentini and Souza 2005), that appear from hydrodynamic instability of currents (Barnier et al., 2011). Propagating eddies transport water mass, heat and large amount of waters rich in nutrients (Fu et al., 2010), and generate dispersion and mixing of isopycnals and density re-stratification (McWilliams 2008). Eddies help structuring marine ecosystems by redistributing plankton and other marine species. Cyclonic (cool) eddies induce the uplift of isotherms (bowl-shaped isolines), thus bringing subsurface waters to lower depths. In the Southern Hemisphere, the cyclonic eddy is represented by a clockwise rotation (Leão 2013).

Some studies have described eddies in the western South Atlantic - Southeast Brazil (Silveira et al., 2000, Calado 2001, Campos 2006, Gabioux 2008, Leão 2013, Newton 2013, Mill et al., 2015). The region between Vitória (~20.5°S) and Cape Frio (~23°S) is depicted by some cyclonic eddies, generated from the meandering of the BC. Receiving intensive scientific attention (Signorini et al., 1989, Silveira et al., 2000, Mata et al., 2012, Pereira et al., 2013, Lima et al., 2016), the BC flows poleward along the shelf break. This western boundary current transports two water masses: the Tropical Water (TW) and the South Atlantic Central Water - SACW. Right underneath the BC, the Intermediate Western Boundary Current (IWBC) carries Antarctic Intermediate Water (AAIW) equatorward (Silveira et al., 2008). The current meandering in this region, and subsequent eddy formation and growth, occurs due to baroclinic instability of the first mode (Silveira et al., 2008, Fernandes et al., 2009, Mano et al., 2009). Although the change in the coastline orientation (Mano et al., 2009) and bathymetric features are also triggering elements to current meandering due to potential vorticity conservation (Campos et al., 1995).

The Southeast Brazil area holds intensive oil and gas exploitation in the continental margin. Therefore, the development of a good forecast, with the ability to predict the mesoscale features is an essential key in cases of oil spill accidents to perform response plans. The skill to understand the ocean dynamics in this region and to produce high quality short-term forecasts is a decisive factor to collaborate with the offshore industry, enabling to plan hypothetical scenarios of influence of an oil spill (Marta-Almeida et al., 2013).

This region contains three key locations that frequently generate eddies: Vitória, Cape Frio and Cape São Tomé (~22°S) (Calado et al. 2010). Although, the Cape São Tomé region has little information on the periodicity and quantities of its eddies. The present study is the initial step toward the construction of an Ensemble Kalman Filter under REMO. This preliminary work tests the model sensitivity to perturbations in the initial condition and atmospheric forcing. This study focuses on the specific event of a cyclonic eddy formed on March 2011 on Cape São Tomé (CST), located off the Brazilian southeast shore around 22°S. The behaviour of this CST eddy has been described in detail by Mill et al. (2015), who analysed 9 years of altimetry data, SST, ocean colour images, XBT and Acoustic Doppler current profiler (ADCP) data. This CST eddy was first noticed around 15 March 2011. According to Mill et al. (2015), this

eddy was completely detached from the Brazil Current in the end of April moving northward, reaching Tubarão Bight one month later, with average speed of approximately 5-7 km day^{-1}, maximum SLA of about 20 cm and a radius of 55 km. This ring is strongly baroclinic, although it presents a large barotropic component, given that it can influence depths of about 800m, which is deeper than the Brazil Current observed depths. Thereby, its northward movement can be driven by the IWBC flow (Mill et al., 2015). The present sensitivity study constructed an ensemble with forty-three 30-day hindcasts initialized on 16 April 2011. A total of 39 members were produced by perturbations in the initial condition, and only 4 by perturbing the atmospheric forcing. In this study, the former members will be referred to as MIC and the latter as MFORC. The CST eddy was tracked following the algorithm proposed by Faghmous et al. (2015) that assumes a cyclonic eddy has a minimum extreme contour of SLA. Other studies have also used this algorithm to detect and track eddies, such as Ashkezari et al. (2016) and Dong et al. (2016).

This manuscript has the following organization. In the next session, the HYCOM+RODAS system is briefly described. In session 3, the numerical experiments within the perturbations are described. Session 4 presents the metrics employed to assess the model sensitivity to the perturbations. In session 5 the results are discussed, and session 6 gives the conclusions.

2 The HYCOM+RODAS system

As a successor to the Miami Isopycnic Coordinate Ocean Model (MICOM) (Bleck et al., 1992), HYCOM is a primitive-equation model that employs a hybrid vertical coordinate system and solves five prognostic equations - two for the horizontal velocity components, the continuity equation, and two conservation equations for a pair of thermodynamic variables as salinity and density and temperature and salinity (Bleck, 2002). The hybrid coordinate (Bleck and Boudra, 1981) is isopycnal (density tracking) for the open, stratified ocean, softly reverting to a terrain-following (sigma) coordinate in shallow coastal regions, and to z-level (constant fixed depths) coordinates in the mixed layer and over unstratified ocean regions. In this process, HYCOM takes the advantages of the three coordinate types by optimally simulating the features in different parts of the ocean: coastal and open-ocean (Chassignet et al., 2007). The model freely adjusts the coordinate type, smoothing the numerical implementation of

some physical processes like mixed layer detrainment and convective adjustment (Chassignet et al., 2006). HYCOM spatial discretization uses Arakawa C-grid, to which temperature, density and salinity are located in the centre of the cells, while the zonal and meridional velocities are located in the East/West and North/South edges of the cells, respectively. Time integration in HYCOM occurs using finite differences through a leapfrog scheme where information from two previous time steps is used to calculate the value of the variables in the desired step.

HYCOM was configured with 1/12° of horizontal resolution, approximately 8 km, with 733 by 601 grid points in the meridional and zonal directions, respectively, over the region 68°W-18°W, 45°S-10°N, comprising the Metarea V. HYCOM was configured with 3 upper vertical layers fixed as z-level coordinate layers with minimum thickness of 3 m and 18 hybrid layers, totalizing 21 vertical layers. The chosen target potential densities were 19.50, 20.25, 21.00, 21.75, 22.50, 23.25, 24.00, 24.70, 25.28, 25.77, 26.18, 26.52, 26.80, 27.03, 27.22, 27.38, 27.52, 27.64, 27.74, 27.82 and 27.88. The first layers have lighter potential density values to preserve a good vertical resolution in the mixed layer. The model was nested in a lower resolution (1/4°) HYCOM assimilative run (Mignac et al., 2015) over almost all the Atlantic Ocean from 78°S to 50°N and from 100°W to 20°E, except the Pacific Ocean, the Mediterranean Sea and the North Atlantic subpolar region. The lateral boundary conditions on HYCOM 1/12° were forced with interpolated velocity fields, temperature salinity and layer thickness from HYCOM 1/4° simulations.

The HYCOM 1/12° grid allows the representation of large- and mesoscale phenomena in the ocean, such as the Brazil Current and its associated eddies. HYCOM makes a dynamically smooth switchover among the coordinate types, regarding the local ocean characteristics, so that considering the entire hybrid system, the 18 isopycnic layers can be turned into sigma- or z-coordinate layers. The model bathymetry was interpolated from the Earth Topography 2 (ETOPO2), with 2-minute resolution, and later adjusted with bathymetric information from the Brazilian Navy. The version 2.2 of HYCOM was used here.

HYCOM 1/4° was initialized from temperature and salinity at rest with the World Ocean Atlas (WOA - 2013), being forced with climatological atmospheric fields from the Comprehensive Ocean Atmosphere Data Set (COADS) and integrated since 31 December 1984 to 2013.

On HYCOM 1/12°, the simulation began on 01 January 1995 from a restart file interpolated from HYCOM 1/4° to 1/12°. From 1995, both domains were forced employing the National Centers for Environmental Prediction/National Center for Atmospheric Research (NCEP/NCAR) reanalysis I (Kalnay et al., 1996). The model generated a positive SST and temperature bias over the long integration period in both HYCOM free runs. This affected the model sea surface height (SSH) and when assimilation of Argo T/S profiles and SST data was realized a reduction in the model SSH mean was produced. The full assimilation run with SST, T/S profiles and SLA data was conducted after a run in which only SST and T/S profiles were performed from 2006 to 2008 (Mignac et al., 2015). The HYCOM+RODAS full assimilation run with the nested system HYCOM 1/4° and HYCOM 1/12° was performed from 2008 to 2013. It was forced with NCEP Climate Forecast System Reanalysis (CFSR) and the Climate Forecast System Version 2 (CFS) analysis fields (Saha et al., 2014). HYCOM was forced with wind speed at 10 m, momentum fluxes, precipitation, temperature and short- and long-wave radiation fluxes at the surface, air temperature and specific humidity at 2 m, sensible and latent heat net fluxes at each 6 h. The HYCOM+RODAS output from this run on 16 April 2011 was used as the control initial condition for the 30-day hindcasts experiments of the present study.

On the present work, RODAS assimilated gridded sea surface temperature data from OSTIA, with 5 km horizontal resolution; gridded sea level anomaly data by Archiving, Validation and Interpretation of Satellite Oceanographic Data (AVISO); and temperature and salinity (T/S) profiles (Tanajura et al., 2014; Costa and Tanajura 2015; Mignac et al., 2015). OSTIA products include a diversity of satellite sensors that measure the infrared and shortwave radiation. They are combined with in situ data to define SST by an Optimal Interpolation scheme, assimilating data in depths equal to or higher than 30 m. A previous interpolation was performed from the OSTIA grid to the model grid. These data were provided by the Group for High Resolution Sea Surface Temperature (GHRSST). AVISO data have 1/4° spatial resolution, calculated from a 1993 to 2012 mean dynamic topography field, representing a composition of the altimeters Envisat, Jason 1 and 2 and Cryosat, using the delayed time product that has better quality control. Concerning the uncertainties of the altimeters in shallower regions, only grid points with depths greater than 300 m were assimilated. On the T/S profiles, different observation data were used: 1) 7081 Argo free-drifting profiles

(http://www.argo.ucsd.edu/), that underwent by a data quality control procedure developed by REMO and the Brazilian Navy; 2) 1072 XBTs (EXpendable BathyThermographs) transects from the high density AX97 radial from a joint program between the Monitoring the upper ocean transport variability in the western South Atlantic (MOVAR) (www.aoml.noaa.gov/phod/hdenxbt/) and the National Oceanic and Atmospheric Administration (NOAA); 3) 267 Conductivity, temperature and density (CTD) profiles by CENPES. The last two in situ data were carefully analysed by CENPES and the XBTs profiles already have a specific data quality control.

2.1 RODAS data assimilation scheme

In this subsession, some details of the EnOI scheme used in RODAS are presented.

The analysis x^a according to the EnOI scheme (Evensen, 2003) is given by:

$$x^a = x^f + K[y - \mathcal{H}(x^f)] \quad (1)$$

$$K = \alpha(\sigma \circ \mathrm{B})H^T[\alpha H(\sigma \circ \mathrm{B})H^T + R]^{-1} \quad (2)$$

$$B \equiv \frac{1}{m-1}AA^T \quad (3)$$

where in Eq. 1 x is the state estimate and the superscripts *f* and *a* refer to forecast and analysis, respectively. The term y is the observation vector; $\mathcal{H}$ is the observation operator. *K* is the Kalman gain matrix, which is responsible for defining the relative importance of the model and the observations to compose the analysis. The term $y - \mathcal{H}(x^f)$ is the innovation vector, which determines the difference between the observation and the model in the space of observations, and $K[y - \mathcal{H}(x^f)]$ is the analysis increment, that determines the impact produced by the assimilation in the prior or background state. In Eq. 2 the term B is the background covariance matrix; H is the linearized observation operator; R is the observation error covariance matrix. The superscript *T* is the matrix transpose. The term α is a scalar that can restrain the magnitude of the analysis increment and $0 < \alpha \leq 1$. The term σ is the localization operator applied over *B* to remove spurious correlations by a Schur product, a multiplication among the elements with the same index in the matrices, represented by

the symbol ∘. In Eq. 3, A is the matrix of background ensemble anomalies; and *m* is the ensemble size. The model background state used in this particular study is the result of the third day of integration after the analysis, since RODAS assimilates data at every 72 hours.

The EnOI method estimates the model error covariance B from an ensemble of model states produced by a long-term free model run. In the assimilation run that lead to the control initial condition employed in the present sensitivity study, 126 model simulations were selected according to the assimilation day. For instance, in the assimilation conducted on 16 April 2011, 21 members centred on 16 April of each year from 2003 to 2007 were taken with three days between each member. Therefore, RODAS does not use a static covariance matrix, since it considers the model intraseasonal-to-seasonal variability. The number of ensemble members and the time interval between each ensemble member taken in the same year of the free run is flexible.

RODAS follows equations 1-3, with assimilation of SST, T/S profiles and SLA conducted separately. At 00 UTC, SST is assimilated aiming to mostly constrain the mixed layer. Three hours later, the T/S profiles are assimilated to correct the model thermohaline structure. Finally, SLA is assimilated at 06 UTC to mainly correct the surface mesoscale features. The control initial condition of the present sensitivity experiment was taken at 09 UTC 16 April 2011. The assimilation of SST, T/S profiles and SLA took about 40 min of wall clock time in 4 nodes of an SGI machine, each node with 16 processors of 2 GHz and 64 GB of RAM memory.

3 Ensemble generation

In this session, the perturbations employed in this sensitivity experiment are described.

On the study area, the forecast errors can be introduced by uncertainties in the initial conditions, atmospheric forcing and model open boundary conditions. The latter was not explored in this work. The 30-day hindcasts were free runs with assimilated initial condition and were performed in order to increase the model spread in a short period through perturbations added on the first day of the integrations. The initial condition was perturbed on 16 April 2011. The ensemble of 30-day integrations was

generated by perturbing the control initial condition through three different strategies, which provided 39 members, and forcing the control initial condition with perturbed atmospheric forcing, creating 4 more members

The three strategies perturbing the control initial condition are called 1) Alpha experiment; 2) Observation error covariance matrix experiment; 3) Standard deviation experiment. The only strategy consisted of perturbing the atmospheric forcing is called 4) Atmospheric forcing experiment. The control initial condition was already assimilated, therefore no new data assimilation was performed to experiments 3 and 4: the perturbation was only added to the control initial condition. To the other strategies, a new data assimilation cycle was performed. The perturbations were computed to every grid point in the HYCOM 1/12° domain. All the 43 members produced with the strategies employed in this study are summarized in Table 1.

3.1 Alpha experiment (Strategy 1)

This strategy employed different values for α (Eq., 2) in every time step of the assimilation cycle. Five integrations were carried out using different values of α: 0.1, 0.3, 0.5, 0.8 and 1.0. These values were employed in the assimilation of all observations to construct five new initial conditions on 16 April 2011. The members of this strategy are called Alpha listed in ascending order from 1 to 5.

3.2 Observation error covariance matrix experiment (Strategy 2)

Assimilation was conducted to produce different initial conditions by considering the observation error covariance matrices R for SST, T/S profiles and SLA data. The entries were increased or decreased by stochastically generated numbers between 1 and 0. Therefore, the new R of Equation 2 were given by:

$$R_{new(i,i)} = R_{(i,i)} \pm R_{(i,i)} \times rand_{num} \quad (4)$$

For each observational point, a different random number was generated. Ten new members with this strategy were created, in which the first (last) five consisted of increasing (decreasing) R. Therefore, different analysis were constructed considering more or less weight on the model background with respect to observations. The members of this strategy are called Error listed in ascending order from 0 to 9 (see Table 1).

3.3 Standard deviation experiment (Strategy 3)

The standard deviation (SD) of the zonal velocity (u), meridional velocity (v) and temperature were calculated from the surface down to the mixed layer of the HYCOM domain. A total of 126 members from the HYCOM+RODAS run were used to estimate the model SD for u, v and T. The members were chosen taking the initial day (16th April) of every year from 2008 to 2013 and 20 members around it, with three days between each member. The final step consisted of adding or subtracting a percentage of the SD of u, v, and T in every grid point in the surface z-layers to the first isopycnal. Therefore, perturbations were inserted mostly in the model mixed layer. In this strategy, 24 members were simulated named SD 11-18, SD 21-28 and SD 31-38, considering 10%, 20% and 100% of the SD values, respectively. Among the 24 members, 18 were produced with u and v perturbations and 6 with temperature perturbations. This strategy naturally excites the model in regions of larger variability and the different percentages will allow to investigate the relation between the magnitude of the perturbation and the spreading.

3.4 Atmospheric forcing experiment (Strategy 4)

The 6-hour CFS products were perturbed to investigate HYCOM sensitivity to the atmospheric forcing. The wind speed and momentum flux were used to create perturbations on the forcing fields. It has been verified that perturbing the wind speed gives good spread in the ocean surface (Hoffman et al., 2012; Shu et al., 2011, Sakov et al., 2012). Thereby, four variables of the CFS products were used in this strategy: the zonal (UGRD) and meridional (VGRD) components of the 10 m wind and the zonal (UFLX) and meridional (VFLX) momentum fluxes at the surface.

First, the control atmospheric forcing outputs were defined as the 6-hour CFS products for the period 16 April 2011 to 15 May 2011. The perturbation consisted of daily anomalies added to every 6-hour wind components and momentum fluxes of the control atmospheric forcing outputs. The daily anomalies of each variable were obtained after subtracting the arithmetic mean calculated for all the 30-day period of the years 2011 to 2014. Therefore, four groups of 30 daily anomalies per year were used as perturbations in the control atmospheric forcing outputs, creating four new

Table 1. Perturbation system applied in this work. SD is the standard deviation; u and v are the zonal and meridional components of the velocity. Anom is the anomaly. UGRD, VGRD, UFLX and VFLX are the zonal and meridional components of the wind and the momentum flux, respectively.

STRATREGY	EXPERIMENT			PERTURBATIONS			TOTAL MEMBERS
Standard Deviation	SD 11	SD 21	SD 31	u+10%SD(u)	u+20%SD(u)	u+100%SD(u)	24
	SD 12	SD 22	SD 32	u-10%SD(u)	u-20%SD(u)	u-100%SD(u)	
	SD 13	SD 23	SD 33	v+10%SD(v)	v+20%SD(v)	v+100%SD(v)	
	SD 14	SD 24	SD 34	v+10%SD(v)	v-20%SD(v)	v-100%SD(v)	
	SD 15	SD 25	SD 35	u+10%SD(u) + v+10%SD(v)	u+20%SD(u) + v+20%SD(v)	u+100%SD(u) + v+100%SD(v)	
	SD 16	SD 26	SD 36	u-10%SD(u) + v-10%SD(v)	u-20%SD(u) + v-20%SD(v)	u-100%SD(u) + v-100%SD(v)	
	SD 17	SD 27	SD 37	T+10%SD(T)	T+20%SD(T)	T+100%SD(T)	
	SD 18	SD 28	SD 38	T-10%SD(T)	T-20%SD(T)	T-100%SD(T)	
Observation error covariance matrix (R)	Error 0-4			Increasing R			10
	Error 5-9			Decreasing R			
Alpha	Alpha 1			α=0.1			5
	Alpha 2			α=0.3			
	Alpha 3			α=0.5			
	Alpha 4			α=0.8			
	Alpha 5			α=1.0			
Atmospheric forcing (AF)	AF1			UGRD/VGRD/UFLX/VFLX 2011= Value + Anom 2011			4
	AF2			UGRD/VGRD/UFLX/VFLX 2011= Value + Anom 2012			
	AF3			UGRD/VGRD/UFLX/VFLX 2011= Value + Anom 2013			
	AF4			UGRD/VGRD/UFLX/VFLX 2011= Value + Anom 2014			

members to the ensemble, called AF1, AF2, AF3 and AF4 (see Table 1).

4 Evaluation metrics

The sensitivity of the model to the proposed ensemble generation was analysed in five steps. First, the temperature and sea level anomaly standard deviation considering all 43 runs were calculated for days 10, 20 and 30 after 16 April 2011. Second, the 43 members were analysed in a “spaghetti” plot, presented in the next section, to investigate spreading of each member in the region of study, comprising the CST eddy. The study area is the southeast Brazil from 24°S-20°S and 42°W-37°W. Third, a cross-section was analysed to investigate whether the perturbations imposed a different temperature, salinity and velocity distribution in the subsurface. Fourth, the eddy tracks for all integrations were captured using the algorithm proposed by Faghmous et al. (2015), hereafter FAG. In the case of a cyclonic eddy, the FAG code would search for a closed-contour of negative SLA with a minimum extreme, defined as a grid cell where there is a decrease in SLA in comparison to its 24 grid, in a 5x5 neighbourhood. The algorithm was applied to identify the eddies in the HYCOM snapshot for all 43 hindcasts given the 1/12° domain. Then, the eddy was tracked in time by associating a feature in the next daily time-step. If there are two subsequent time-steps that have no information of the SLA minimum, the track is terminated. Fifth, the temperature distribution from the surface down to bottom of every latitude/longitude point of each track was extracted in order to analyse the spreading in the centre of the eddy. The ensemble spreading of the position of the 20°C and 22°C isotherms were analysed in depth, as for the standard deviation of the temperature given target depths.

Before evaluating the spreading, it is important to analyse how the model can respond to the perturbation strategies. The model response to the members with perturbed initial conditions is due to the data assimilation system or the ocean model parametrization. If there is an increase (decrease) of the observation error covariance matrix or analysis increment, the analysis gives more weight to the background (observational data). The perturbation with the standard deviation (Section 3.3) will more efficiently affect areas of greater variability. The model response to the members with perturbed atmospheric forcing is given by the close response of the ocean surface to wind forcing through the perturbations, since other atmospheric parameters were not perturbed when compared to the control forcing outputs.

5 Results and discussion

Figure 1 shows the spatial distribution of SLA (left panel) for AVISO, the control, and two members of the ensemble (Error 9 and AF1, see table 1) and SST (right panel) for OSTIA, the control run and the same ensemble members mentioned above (Error 9 and AF1) on 08 May 2011. In comparison with the observations and the control, both Error 9 and AF1 kept the SLA and SST signal of the eddy at the surface, although its position is given at different locations, to the north or south of 22°S, and they present different shapes of the eddy. This result shows that the ensemble of hindcasts have an impact on generating variance or spread in the position, shape and size of the eddy.

Even though the model has a temperature bias, the Error 9 SST field is warmer than the OSTIA field, the AF1 member shows a cooler distribution of the SST, which can be a response of the surface temperature to the perturbations in the wind speed and momentum fluxes on this member. The cooler SST distribution in the AF1 member can be explained by the close relation among momentum fluxes, sensible and latent heat fluxes and wind speed. The increased wind speed imposed in the AF1 member would cause an increase in the sensible and latent heat fluxes and, consequently, cooling of the ocean surface.

The cooler SST was observed in all the perturbed atmospheric forcing members in which u and v were increased. Near Cape São Tomé, cyclonic eddies from the BC are important features to the development and enhancement of the coastal upwelling system in this area (Calado et al., 2010). The SST presented cooler values in the continental shelf region for all the members and for the control and OSTIA fields. This can be explained by the prevailing NE winds that induce coastal upwelling with intrusion of SACW into this region.

The AF1 temperature and meridional rotated velocity component sections on 08 May 2011 are presented in Figure 2. The cross section is the solid black line presented in Figure 1. The sections characterize the CST cyclonic eddy, which causes lifting of the isotherms in a convex shape. The cyclonic eddy is positioned between 39°W and 38°W, as it is shown in the SLA field for the AF1 member in Figure 1. Figure 2b shows a strong barotropic component of the CST eddy. The positive velocities (red) are northward and negative velocities (blue) a southward flow.

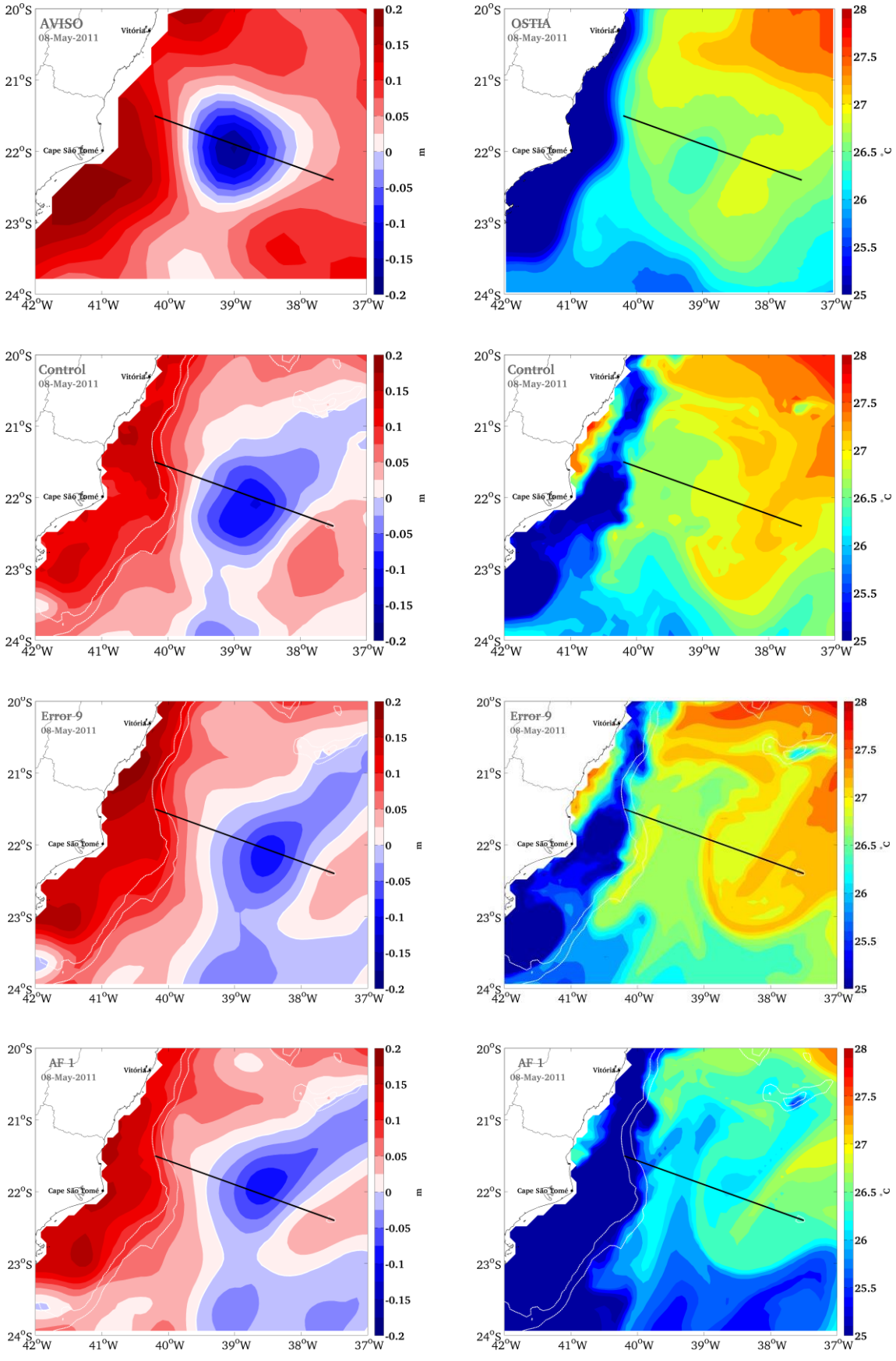

Figure 1. Sea level anomaly (left panel) field for the AVISO, the control run, Error 9 and AF 1 ensemble members and sea surface temperature (right panel) distribution for OSTIA, the control run, Error 9 and

AF1 ensemble members on 08 May 2011. The white dashed lines represent the 200 m and 1000 m isobaths (presented by HYCOM) indicating the location of the continental shelf and slope. The solid black line represents a cross section in the study area.

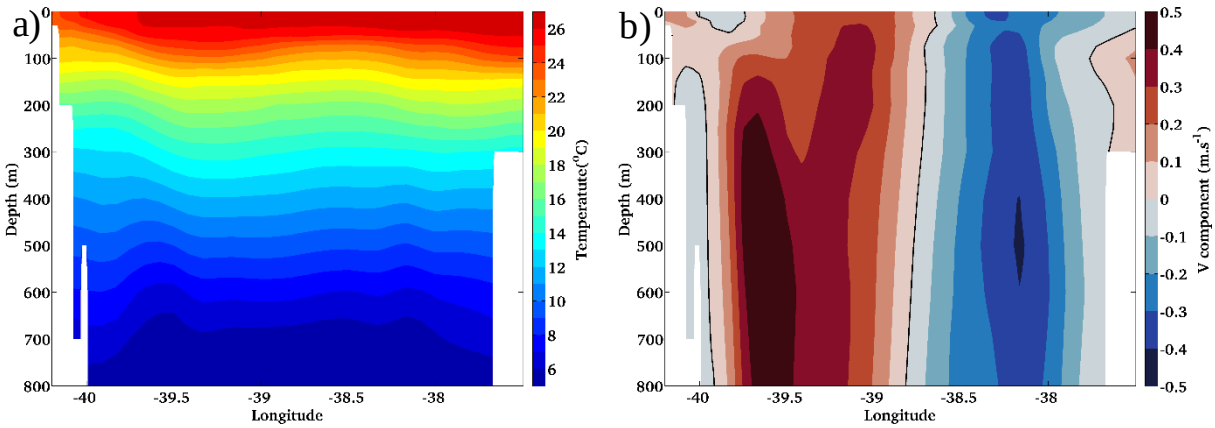

Figure 2. Cross section through the Cape São Tomé cyclonic eddy taken on 08 May 2011 showing (a) the temperature structure in °C and (b) meridional velocity component structure down to 800 m for the AF1 ensemble member.

The perturbation system did not affect the maximum deformation of the isotherms that is around 100 m as described by Mill et al. (2015). The section does not necessarily cross the eddy centre for all members, but they display close distributions for temperature and velocity inside the eddy. The cold core eddy can be felt in depths of 800 m or higher, although near the surface, the temperature is almost the same inside the eddy and in its vicinity, as found by Mill et al. (2015). The eddy is also less saline.

The temperature standard deviation among the 43 ensemble members in the cross section on 08 May 2011 is presented in Figure 3. The greater variability of the ensemble was observed in the first 200 m of the section. It is due to the model response to the perturbations that occurred down to the first isopycnal layer and a near-surface response to the atmospheric forcing members. In depths greater than 400 m, the SD presented the lowest values for temperature, velocity and salinity (not shown). The area of greater temperature SD is located around 40°W, in the upper 100 m of the water column. The section highest SD value was 0.61°C in about 30 m, which can be a result of the cooler waters, especially in the slope area, showed to the SST distribution of the AF1 member. Below 400 m, the SD was lower than 0.05 °C (not

shown). The high SD values found around 100 m between 38°W-39°W could be a representation of the difficulty of ocean models to depict the sharpness of the thermocline region (Oke and Schiller 2007, Xie and Zhu 2010). The greater SD for salinity and zonal and meridional velocity components (not shown) were highest near the surface, with values of 0.10, 0.08 $m.s^{-1}$ and 0.09 $m.s^{-1}$, respectively.

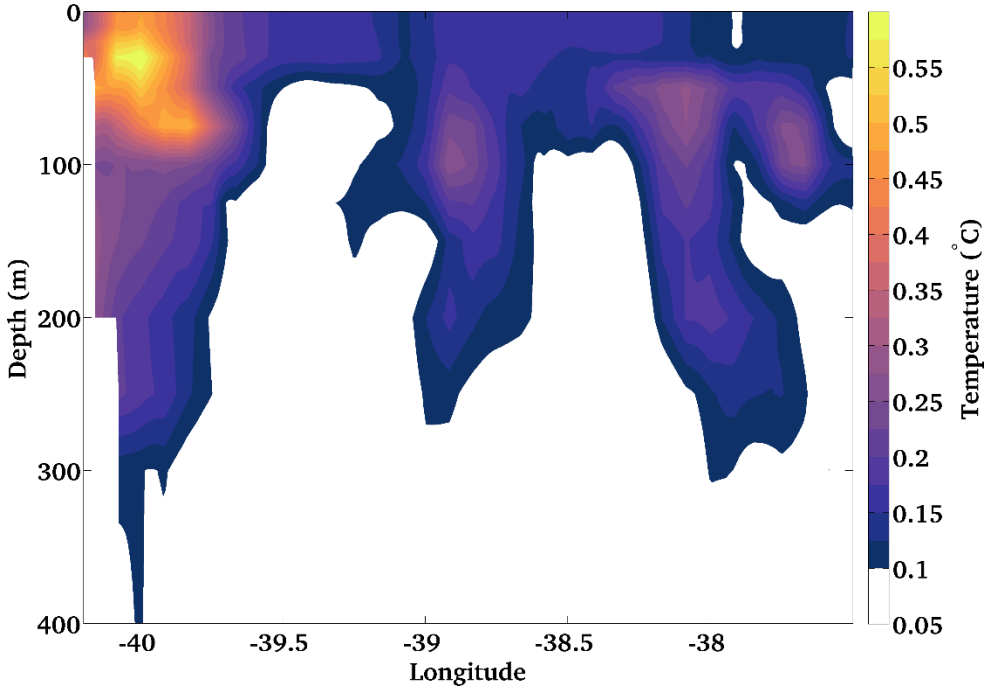

Figure 3. Cross section showing the temperature standard deviation from the surface down to 400 m among the 43 ensemble members on 08 May 2011.

The ensemble spreading for the HYCOM 1/12° domain is presented in Appendix A. The temperature and sea level anomaly SD in the study region is given on Figures 4 and 5. The SD was calculated among all the ensemble members on days 10, 20 and 30. Throughout time, the SD at the surface increased for both SST and SLA. The area averaged T SD at the surface were 0.18°C, 0.19°C and 0.23°C on days 10, 20 and 30, respectively. The highest SD for the SST were 0.84°C, 0.49°C and 0.54°C for days 10, 20 and 30, respectively. At 50 m (Figure 5b), the largest SD were 0.92°C, 1.29°C and 1.89°C and the area averaged SD was 0.17°C, 0.25°C and 0.25°C for days 10, 20 and 30, respectively. At 100 m (Figure 5c) the maximum SD values were 1.05°C, 0.99°C and 1.40°C and the area averaged SD values were 0.13°C on day 10, 0.18°C on day 20, and 0.21°C on day 30. At the surface, there was an increase from day 10 to day 30 of approximately 27.7% in the mean SD, followed by the subsurface, although it did not have a great increase in area as for the surface. The SST does not have larger

deviation at the surface as a response to the air temperature, which was not perturbed in this work.

The highest SLA standard deviation values found (Figure 6) for days 10, 20 and 30 were 0.027 m, 0.044 m and 0.047 m, respectively. The domain averaged SD values on Figure 6 were 0.007 m, 0.009 m and 0.01 m on days 10, 20 and 30, respectively. The increase in the mean SLA SD was about 42.8% throughout the 30 days. In the continental shelf, the ensemble attained the highest SD values for both SST and SLA. It is probably due to stronger variability associated with coastal processes. Although the model already has a temperature and SLA bias near the coast on the study region.

Table 2 shows the T on the surface, at 50m and 100 m and SLA standard deviation for each strategy, calculated in relation to the ensemble mean. The standard deviation was calculated for each strategy on days 10, 20 and 30. Overall, for both temperature and SLA, the MFORC members (strategy 4) had the largest SD among all strategies. For instance, the highest SD on day 30 was produced at 50 m depth for all the 43 members. However, the main SD contribution came from the MFORC members, corresponding to 6.28°C, followed by 1.81°C with the strategy 2, 1.12°C with strategy 1 and 0.97°C with strategy 3. In respect to the mean T SD, the main contribution came from strategy 4 with 0.710°C, followed by 0.192°C with the strategy 2, 0.147°C with the strategy 1 and 0.140°C with the strategy 3. Although, the highest SD mean was to Strategy 4 on the surface on day 30. Therefore, MFORC had the greatest contribution to cause spreading in respect to both highest and mean SD values in the study area. Strategy 2 (observation error covariance matrix experiment) was the second largest contribution to the highest and mean SD, followed by strategy 1 (alpha experiment) and strategy 3 (standard deviation experiment), except for the SST SD on day 30, where the second largest contribution was given for strategy 3, followed by strategy 2 and strategy 1.

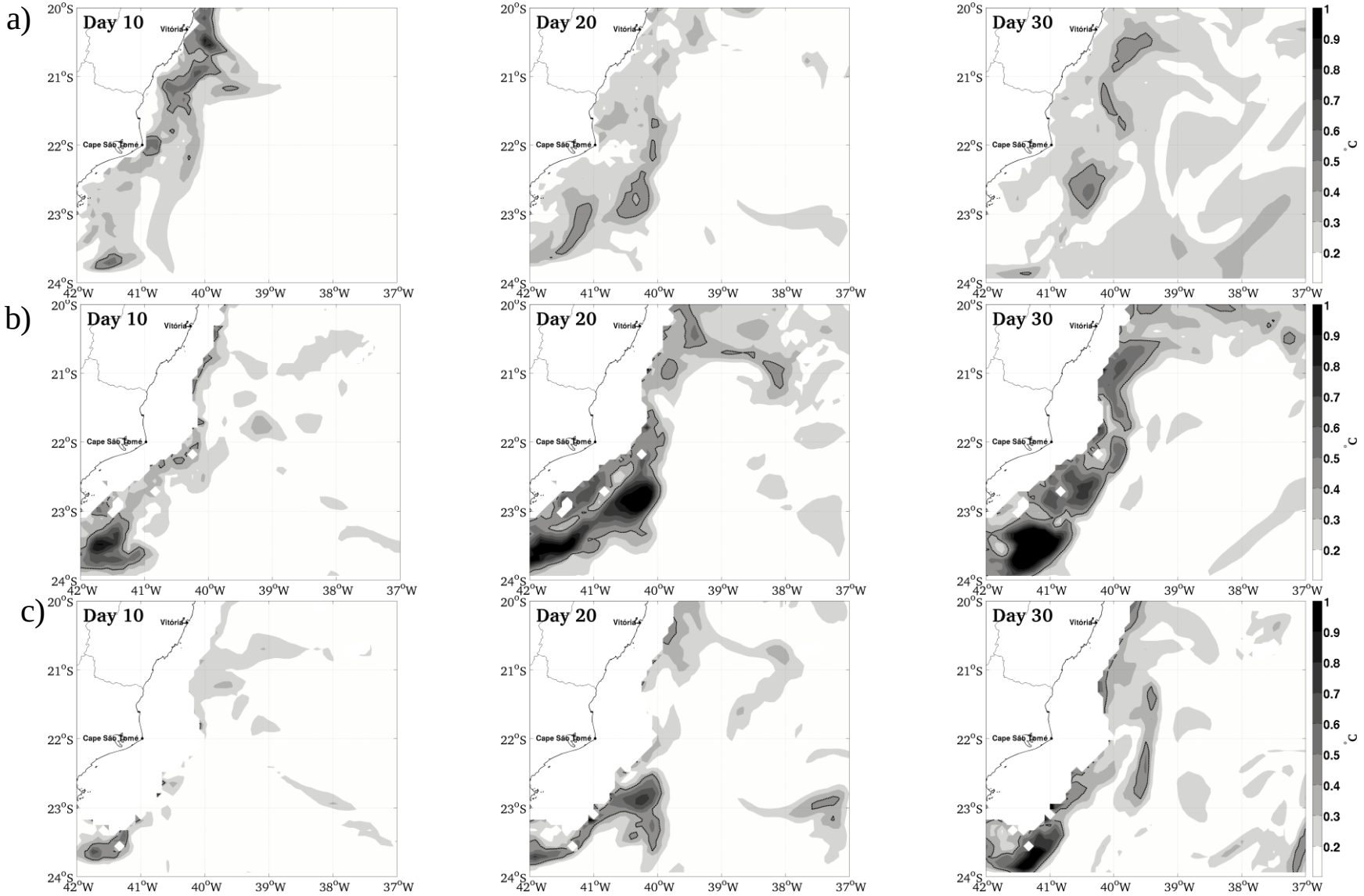

Figure 4. Temperature standard deviation for days 10, 20 and 30 at (a) the surface, (b) 50 m and (c) 100 m depth. The dashed black line represents the standard deviation of 0.4°C. The greater standard deviation values are near the Cape São Tomé area.

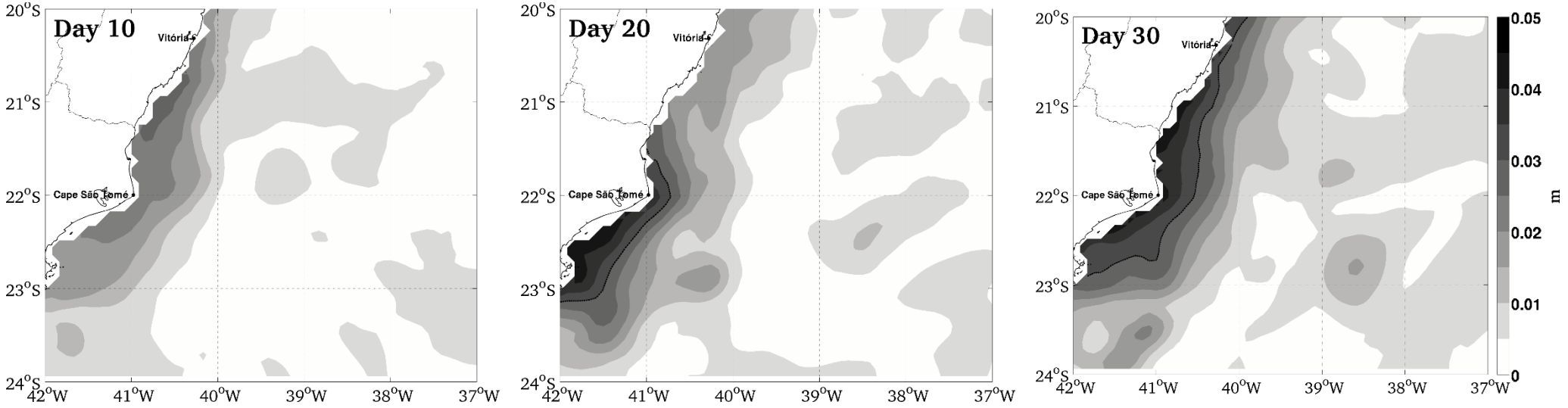

Figure 5. Sea level anomaly standard deviation (in m) among the 43 members. The black dashed line represents SLA standard deviation of 0.03 m.

Table 2. Temperature (in °C) and sea level anomaly (in m) standard deviation on the study area of each strategy in comparison with the ensemble mean. The standard deviation of each strategy was calculated days 10, 20 and 30. Strategy 1 is the alpha experiment. Strategy 2 is the observation error covariance matrix experiment. Strategy 3 is the standard deviation experiment. Strategy 4 is the atmospheric forcing experiment. The standard deviation approximate values show the highest and mean SD values, respectively.

	DAY 10	DAY 20	DAY 30
Sea surface temperature	**Strategy 1:** 0.44 / 0.044 **Strategy 2:** 0.86 / 0.056 **Strategy 3:** 0.54 / 0.145 **Strategy 4:** 3.00 / 0.470	**Strategy 1:** 0.65 / 0.064 **Strategy 2:** 0.66 / 0.072 **Strategy 3:** 0.30 / 0.117 **Strategy 4:** 1.72 / 0.592	**Strategy 1:** 0.64 / 0.097 **Strategy 2:** 0.71 / 0.107 **Strategy 3:** 0.37 / 0.117 **Strategy 4:** 1.90 / 0.757
Temperature at 50 m depth	**Strategy 1:** 0.70 / 0.087 **Strategy 2:** 1.42 / 0.128 **Strategy 3:** 0.85 / 0.126 **Strategy 4:** 2.63 / 0.433	**Strategy 1:** 1.67 / 0.137 **Strategy 2:** 1.30 / 0.169 **Strategy 3:** 1.18 / 0.142 **Strategy 4:** 4.68 / 0.700	**Strategy 1:** 1.12 / 0.147 **Strategy 2:** 1.81 / 0.192 **Strategy 3:** 0.97 / 0.140 **Strategy 4:** 6.28 / 0.710
Temperature at 100 m depth	**Strategy 1:** 1.15 / 0.090 **Strategy 2:** 1.12 / 0.137 **Strategy 3:** 0.98 / 0.064 **Strategy 4:** 2.02 / 0.307	**Strategy 1:** 1.48 / 0.132 **Strategy 2:** 0.84 / 0.172 **Strategy 3:** 0.86 / 0.091 **Strategy 4:** 2.82 / 0.487	**Strategy 1:** 1.67 / 0.149 **Strategy 2:** 2.11 / 0.206 **Strategy 3:** 1.25 / 0.107 **Strategy 4:** 3.53 / 0.519
Sea level anomaly	**Strategy 1:** 0.013 / 0.0031 **Strategy 2:** 0.020 / 0.0040 **Strategy 3:** 0.008 / 0.0032 **Strategy 4:** 0.098 / 0.0212	**Strategy 1:** 0.015 / 0.0037 **Strategy 2:** 0.018 / 0.0053 **Strategy 3:** 0.015 / 0.0035 **Strategy 4:** 0.158 / 0.0275	**Strategy 1:** 0.017 / 0.0047 **Strategy 2:** 0.035 / 0.0070 **Strategy 3:** 0.012 / 0.0033 **Strategy 4:** 0.169 / 0.0356

Figure 6 shows the time series of the ensemble spreading for SST, sea level anomaly, current velocity components and salinity for the study area. Figures 6c, 6d and 6e show the highest values of the meridional and zonal velocity components and salinity, respectively, encountered for each model grid point within the study area of all 43 integrations. The S highest values of the model states are probably located in the halocline regions. Figure 6b shows the daily SLA minimum in the study area for each member, in order to see the spreading in the eddy area, since the SLA minimum would represent the eddy core. Overall, the perturbations of atmospheric forcing have greater impact on the ensemble spread. The variance for the members from perturbed initial conditions do not seem to create major disturbances in HYCOM. It indicates that perturbations in the atmospheric forcing can increase the ensemble spread in the lead-time of 30 days, even if the members have smaller differences on day 1, as seen in Figures 6a, 6b and 6e. The ensemble mean is mostly defined by the behaviour of the members from perturbed initial conditions because they are in larger number. Therefore, if only few of these members are taken, the ensemble mean would lead to another trajectory.

Salinity spreading is given by the initial condition and atmospheric forcing perturbations, although they have little direct impact in the salinity. Since salinity is not directly perturbed in this work, the spreading is a response to the perturbations in the temperature, and velocity. Figures 6c and 6d show that the spreading of MIC is greater around the first ten days but they hardly contribute to the covariance in the end of the 30 days. The same result was found for the study area averaged ensemble members at the surface, when compared to the subsurface (not shown). At the surface, the hindcasts are prone to be dominated by the atmospheric forcing rather than initial condition (Hurlburt et al., 2009). It is possible to affirm that the ensemble settled here is good, since the mean temperature of all ensemble members at the surface is close to the SST observation data from OSTIA (Figure 6a), especially in the final days of the integration. For MFORC, the spreading gets larger with time. This is another indication of the importance of this strategy to construct an ensemble of ocean forecasts. It also shows the time to saturate the forecast error in the ocean is not reached on 30 days of forecasts. As found by Shu et al. (2011), the spreading for MIC has an important role to produce the initial ensemble, and MFORC are responsible for maintaining and enhancing the spreading.

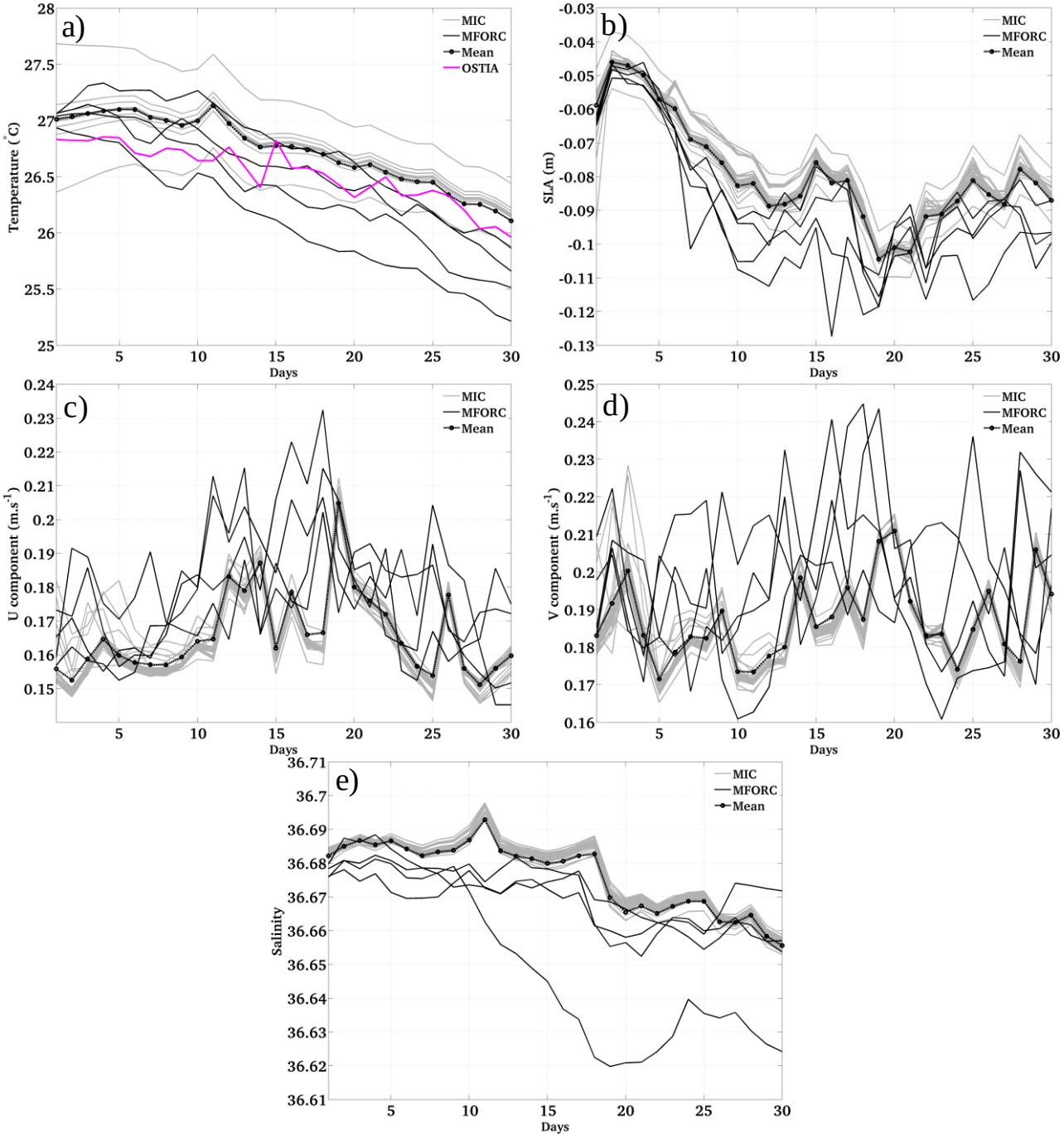

Figure 6. Ensemble spread of the (a) temperature (°C), (b) sea level anomaly (m), (c) zonal velocity ($m.s^{-1}$), (d) meridional velocity ($m.s^{-1}$), and (e) salinity. The grey lines represent the 39 members with perturbations in the initial condition (MIC), and the solid black lines the 4 members from perturbed atmospheric forcing (MFORC). The black dashed line with circle markers is the ensemble mean. The magenta solid line is the SST for OSTIA.

Figure 7 shows the eddy tracking for each of the ensemble members following the FAG algorithm. The tracks are plotted for the cyclonic eddies found by the code for the entire time series, in order to analyse the different positions attained by the eddy core along 30-day forecast window. The tracks are not continuous from day 1 to day

30 for any of the ensemble members. This is a result of the eddy loss of signal at the surface along the 30 days, following the definition of cyclonic eddy in FAG. For all members, the FAG algorithm lost signal at the surface at some day, especially between the third and the fifth day of the hindcasts. By the end of 30 days (Figure 7, black squares), the ensemble spread was enlarged considering the position of the eddy core. MFORC (red lines) influenced the eddy to be positioned in a northward location when compared to MIC (blue lines), which showed a location to the south of the domain. The mean of the eddy tracks of all the 43 members would probably be the best track the model would represent (Kalnay 2003) to this specific event. However, the eddy tracking performed for AVISO (black thick line) showed a position of the eddy track further west of the ensemble members tracks and presented a more linear movement along the 30 days.

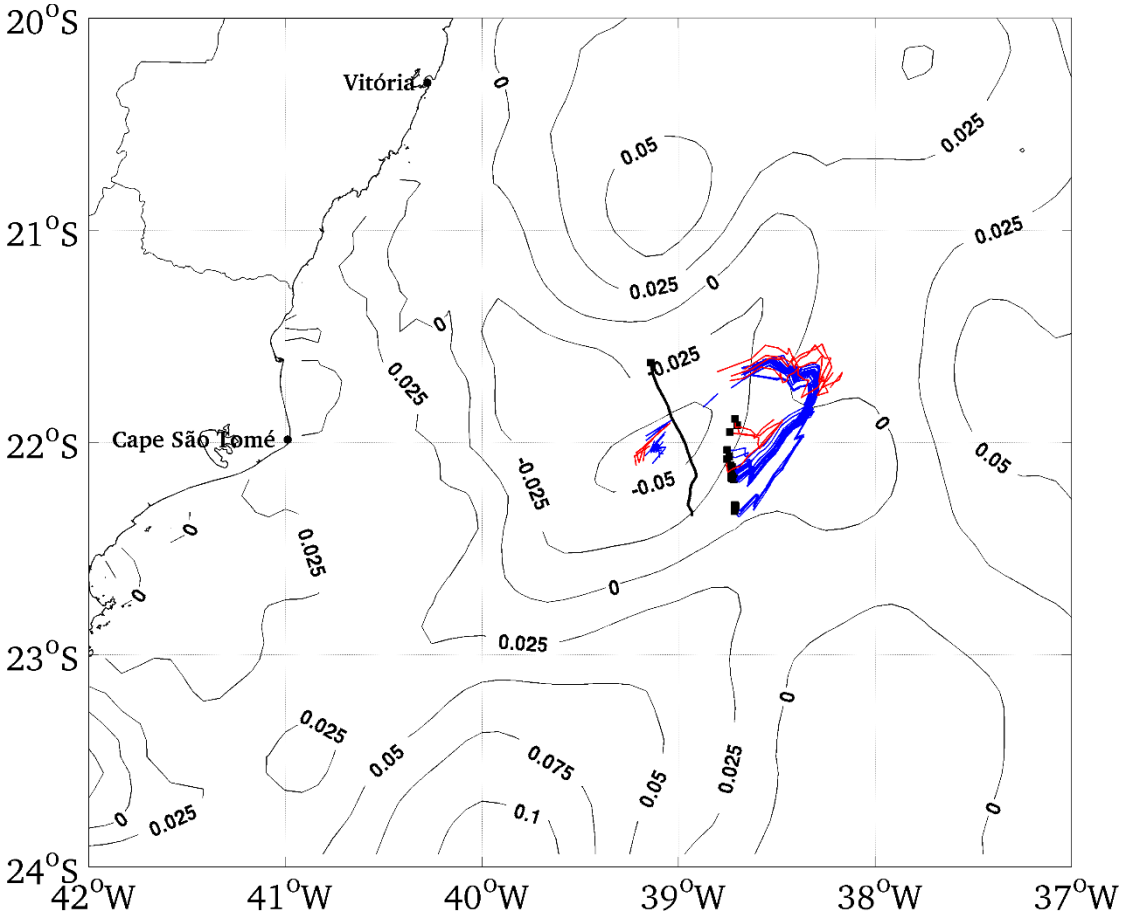

Figure 7. The black filled-in squares represent the tracks in the end of 30 days. The blue solid lines are for the members with perturbed initial conditions, and the red solid lines are the members with perturbed atmospheric forcing. The black line is the AVISO track. The background contour lines show the sea level anomaly (in m) on 16 April 2011 for SD 11 experiment.

The temperature structure in the centre of the CST eddy was analysed for the 30-day lead-time. Figure 8a shows the temperature ensemble spreading in the eddy core at the surface (magenta error bars), at 50 m (black error bars) and 100 m (blue error bars). At the surface, the highest standard deviation found was 0.23°C in the end of the integration days. The minimum SD was 0.14°C on day 9. At 50 m, the maximum SD found was 1.54°C on day 3 and the minimum was 0.07°C on day 1. The highest and lowest SD values at 100 m were 1.39°C and 0.05°C on days 3 and 5, respectively. Figure 8b shows the 22°C (black error bars) and 20°C (grey error bars) isotherms – characterizing the Tropical Water (Pereira et al., 2014) - ensemble spreading with depth for every track position for the entire period. For the 22°C isotherm, the maximum SD found was 22.19 m on day 3 and the minimum SD was 0.67 m on day 5. The analysis of the 20°C isotherm shows a maximum SD of 23.18 m on day 3 and a minimum of 1.36 m on day 24.

It is important to remember that the FAG code did not necessarily found a continuous eddy track for the 30 days of integration. In most of the members, the eddy was fully tracked from day 6 to day 30. In others the tracking was divided into two or even three different tracks (Figure 7). Therefore, on some days there was no eddy to track in some integrations. Most of the initial condition members did not show the CST eddy from day 3 until day 6. This can be a result of the higher SD values throughout these days in the subsurface. Recall that the initial condition members have higher spreading for the subsurface than to the surface (Figure 6). This is a response of the model sensitivity to the atmospheric forcing at the surface (Hurlburt et al., 2009).

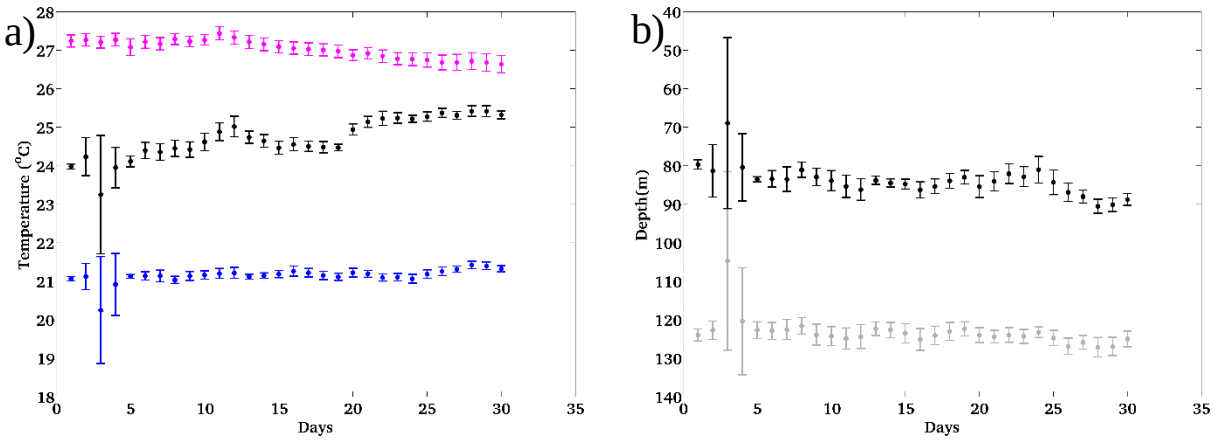

Figure 8. Temperature structure for each point of the eddy tracking for all the ensemble members. Temperature standard deviation (a) in depth at the surface (magenta error bars), 50 m (black error bars)

and 100 m (blue error bars) and (b) following the 22°C isotherm (black error bars) and 20°C (grey error bars).

According to Mill et al. (2015), near the surface the temperature could be almost the same inside and outside the eddy, although the perturbation system in some of the members could bring cooler waters to lower depths and give these results. Analysing Figure 9a, the greater SD on days 3 and 4 in 50 m and 100 m can be explained by Figure 9b, which shows the 22°C isotherm reaching depths of about 48 m in some ensemble member. This can be a result of the isotherms movement in the centre of the eddy. This can be seen in Figure 9.

Figure 9 shows the temperature distribution underneath the track position for the ensemble members that have a minimum SLA closed-contour on days 3 (Figure 9a) and 30 (Figure 9b) according to FAG. It is possible to see that for MIC (grey solid lines on Figure 9a) the temperature was colder than for MFORC (black solid lines on Figure 9a). The highest differences on the T were for the depths around 50 m and 150 m. This could be due to the isotherm uplifting to lower depths to MIC while it did not happened to MFORC on day 3. By the end of 30 days, the temperature spreading inside the CST eddy was already collapsed for all the ensemble members.

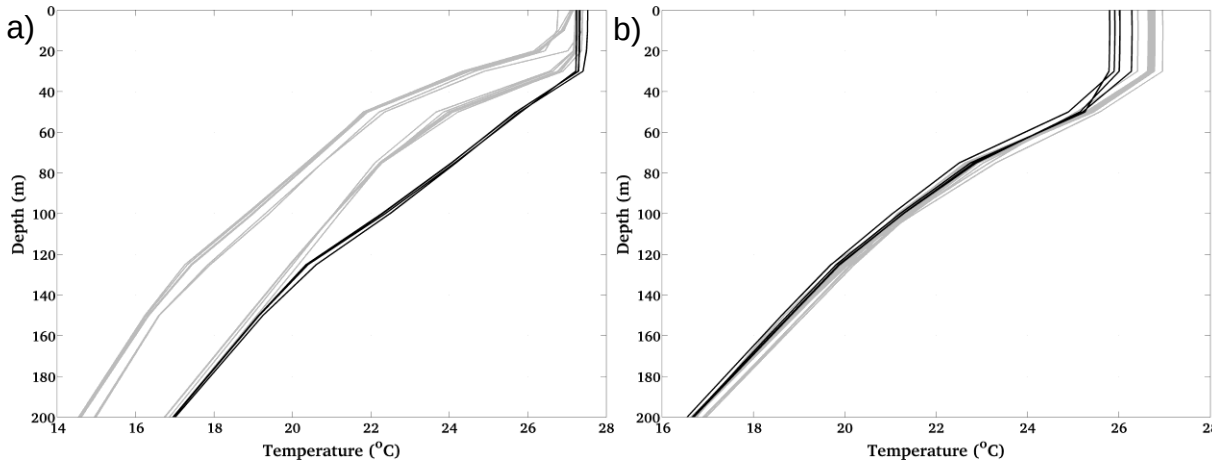

Figure 9. Temperature distribution from the surface down to 200 m (in °C) within the CST eddy for all the members on day 3 (a) and day 30 (b). Grey solid lines are the members with perturbed initial condition and black solid lines represent the integrations with perturbation in the atmospheric forcing.

6 Summary

In this work, an ensemble of hindcasts was applied to investigate the HYCOM model sensitivity to perturbations in atmospheric forcing and initial condition. Different

strategies were employed in order to exploit the best way to produce an ensemble forecast, and in a near future, construct an EnKF data assimilation scheme as an improved version of the REMO Ocean Data Assimilation System (RODAS), based on the EnOI scheme.

In order to assess the model behaviour, forty-three ensemble members were produced using HYCOM for the period of 16 April 2011 to 15 May 2011. This period was chosen to evaluate the effect of the perturbations in a specific cyclonic eddy that pinched off the Brazil Current in late April 2011 (Mill et al., 2015) in the Campos Basin region (20°S-24°S/37°W-42°W). This area has large economic interest, with intensive petroleum exploitation, which is an essential factor for operational oceanography to predict as accurately as possible the state of the ocean through data assimilation. Moreover, an ensemble-based data assimilation system gives an optimal estimate of the model and forecast uncertainties, and the mean among the ensemble members would be the best product a model could offer (Kalnay 2003).

In the ocean, the most important error sources are in the initial condition and atmospheric forcing to estimate the background error covariance matrix using EnKF (Turner et al 2008). The ensemble members were produced according to four strategies: three different strategies perturbed the initial conditions and one strategy perturbed the atmospheric forcing. Two strategies with perturbation in the initial condition were conducted by constructing different analysis with RODAS and for the other the perturbation in the initial condition was constructed by adding perturbation to the control initial condition based on the standard deviation of the temperature, zonal and meridional velocities. The standard deviation for temperature and velocity components were calculated considering 126 model states from a free model run of HYCOM and they were added or subtracted for each corresponding variable. The perturbed atmospheric forcing strategy considered daily anomalies of wind and momentum fluxes obtained from CFS atmospheric analysis from 2011 to 2014. A time series of anomalies were calculated by subtracting the analysis mean from the analysis at each 6h. The anomalies were added to the 2011 analyses from 16 April to 15 May 2011. To generate the ensemble, the four strategies yielded 39 ensemble members with perturbed initial condition, and 4 members with perturbed atmospheric forcing.

The SLA and SST fields imposed different shapes and positions of the cyclonic eddy, depending on the ensemble member. Also, the temperature at the surface and subsurface showed cooler distribution for the members with perturbed atmospheric forcing than for the members with perturbed initial conditions due to the increase of the wind speed imposed in MFORC.

The impact of the different perturbation strategies was evaluated by observing the spreading among the different ensemble members in the 30-day hindcasts. The standard deviation in a cross section was calculated for all the ensemble members to analyse the spreading on temperature with depth. This result showed that the SD is greater in the first 200 m, with the highest values in the first 100 m and closer to the slope area. This could be a model response to the intensification of the 10 m wind velocity that imposed stronger latent and sensible heat fluxes and cooled SST. The cross section also showed that the signal of the eddy in subsurface waters was not lost with the perturbations.

The domain standard deviation for temperature and SLA was also assessed for days 10, 20 and 30. The SD field increased at the end of the 30 days for both SLA and SST, with higher values near the coast and in shallower waters. This can be associated with the larger variability produced by coastal processes and directly influenced by the continental shelf. The SLA and temperature SD on day 30 were also calculated for each strategy separately, in relation to the ensemble mean. For both SLA and T, results showed a higher influence on the SD for the members with perturbed atmospheric forcing, followed by the observation error covariance matrix experiments, alpha experiments and standard deviation experiments.

The ensemble spread in the study area for temperature, SLA, salinity and velocity components was also analysed. Overall, results showed the spreading is greater in the members with perturbed atmospheric forcing throughout the integration time than in the perturbed initial condition members. Although on the first days, the spreading can be greater to MIC than to MFORC, the spreading produced by different atmospheric forcing dominated afterwards.

The CST eddy was tracked following the Faghmous et al. (2015) algorithm. The code showed different tracks for every member, and by the end of 30-day window, the

core of the eddy was at different locations. This shows that there is a significant impact of the perturbation strategies in exciting the model variability. The temperature structure was also analysed for each eddy track point. Results showed a spreading in the temperature distribution in the centre of the eddy, at different depths, regarding the uplifting of the isotherms.

The error source imposed on the atmospheric forcing produced the main contribution to the ensemble spread and covariance in the entire three-dimensional space. Although, the perturbed initial condition members had a good impact in the first days, the spreading was soon diminished. Hence, to this specific event located in southeast of Brazil, to achieve the best variance on 30 days, the EnKF in the region studied should be started with perturbations in the atmospheric forcing.

Acknowledgements

The authors would like to thank CNPq for the fellowship on Scientific Initiation (100207/2017-0) and for the grant provided by Edital Universal 14/2014, process 446528/2014-5. The author would like to thank M.Sc. Filipe. B. Costa for the fundamental support to integrate HYCOM 1/12° within the Brazilian Oceanographic Modelling and Observation Network (REMO) at UFBA.

References

ASHKEZARI, M. D., HILL, C. N., FOLLETT, C. N., FORGET, G., FOLLOWS, M. J. 2016. Oceanic eddy detection and lifetime forecast using machine learning methods. Geophysical Research Letters, 43(23).

BARNIER B, PENDUFF T, LANGLAIS C., 2011. Eddying vs. Laminar Ocean Circulation Models and Their Applications. In: A. Schiller, G. B. Brassington (Eds.), Operational Oceanography in the 21st Century. Springer, Netherlands, pp.239-262.

BELL M, SCHILLER A, LE TRAON P-Y, SMITH NR, DOMBROWSKY E, WILMER-BECKER K., 2015. An introduction to GODAE OceanView. Journal of Operational Oceanography, 8 (1): 2-11.

BLECK R., 2002. An oceanic general circulation model framed in hybrid isopycnic-Cartesian coordinates. Ocean Modelling 4:55-88.

BLECK R, BOUDRA DB. 1981. Initial testing of a numerical ocean circulation model using a hybrid quasi isopycnal vertical coordinate. J. Phys. Oceanogr., 11: 755–770.

BLECK R, ROOTH C, HU D, SMITH LT., 1992. Salinity-driven thermocline transients in a wind- and thermohaline-forced isopycnic coordinate model of the North Atlantic. J. Phys. Oceanogr., 22:1486–1505.

BRYAN FO., 2008. Introduction: Ocean Modeling—Eddy or Not. In Ocean Modeling in an Eddying Regime. Eds M. W. Hecht and H. Hasumi, American Geophysical Union, Washington, D. C., 1-3.

BURGERS G, van LEEWN P J, EVENSEN G., 1998. Analysis scheme in the ensemble Kalman filter. Mon. Wea. Rev.126:1719-1724.

CALADO L., 2001. Dinâmica da formação de meandros e vórtices da Corrente do Brasil ao largo do Sudeste Brasileiro. Master thesis work. Universidade de São Paulo, São Paulo. Portuguese., 112p.

CALADO L, SILVEIRA ICA, GANGOPADHYAY A, DE CASTRO BM., 2010. Eddy-induced upwelling off Cape São Tomé (22°S, Brazil). Continental Shelf Research 30: 1181-1188.

CAMPOS E., 2006. Equatorward translation of the Vitoria Eddy in a numerical simulation. Geophysical Research Letters, L22607, 33(22):5.

CAMPOS EJD, GONÇALVES JE, IKEDA Y., 1995. Water Mass Characteristics Geostrophic Circulation in the South Brazil Bight-Summer of 1991. J. Geophys. Res., 100(9):18537-18550.

CHASSIGNET E, HURLBURT H, METZGER E, SMEDSTAD OM, CUMMINGS J, HALLIWELL G, BLECK R, BARAILLE R, WALLCRAFT A, LOZANO C et al., 2009. US GODAE: Global Ocean Prediction with the HYbrid Coordinate Ocean Model (HYCOM). Oceanography 22:64-75.

CHASSIGNET EP, HURLBURT HE, SMEDSTAD OM, HALLIWELL GR, HOGAN PJ, WALLCRAFT AJ, BARAILLE R, BLECK R., 2007. The HYCOM (Hybrid Coordinate Ocean Model) data assimilative system. J. Marine Syst. 65:60-83.

CHASSIGNET EP, HURLBURT HE, SMEDSTAD OM, HALLIWELL GR, HOGAN PJ, WALLCRAFT AJ, BLECK R., 2006. Ocean Prediction with the Hybrid Coordinate Ocean Model (HYCOM). In: Chassignet, E. P., Verron J. (Eds) Ocean Weather Forecasting. Springer, Dordrecht. 413-426.

COSTA F, TANAJURA C., 2015. Assimilation of sea-level anomalies and Argo data into HYCOM and its impact on the 24 hour forecasts in the western tropical and South Atlantic. Journal of Operational Oceanography 8: 52-62.

DOMBROWSKY E, BERTINO L, BRASSINGTON G, CHASSIGNET E, DAVIDSON F, HURLBURT H, KAMACHI M, LEE T, MARTIN M, MEI S et al., 2009. GODAE Systems in Operation. Oceanography 22: 80-95.

DONG, D., BRANDT, P., SCHUTTE, F., YANG, X., LI, Z. 2016. A new eddy detection method with object segmentation strategies for satellite altimetry. In Geoscience and Remote Sensing Symposium (IGARSS), 2016 IEEE International (pp. 5827-5830).

EVENSEN G., 2003. The ensemble Kalman Filter: theoretical formulation and practical implementation. Ocean Dynamics, 53:343-367.

EVENSEN G., 1994. Sequential data assimilation with a nonlinear quasigeostrophic model using Monte Carlo methods to forecast error statistics. J. Geophys. Res. 99 (C5):10143-10162.

FAGHMOUS J, FRENGER I, YAO Y, WARMKA R, LINDELL A, KUMAR V., 2015. A daily global mesoscale ocean eddy dataset from satellite altimetry. Scientific Data, 2:150028.

FERNANDES A, Silveira ICA, CALADO L, CAMPOS E, PAIVA A., 2009. A two- layer approximation to the Brazil Current–Intermediate Western Boundary Current System between 20°S and 28°S. Ocean Modelling, 29(2):154-158.

FU L-L, CHELTON DB, LE TRAON P-Y, MORROW R., 2010. Eddy dynamics from satellite altimetry. Oceanography 23(4):14–25.

GABIOUX M., 2008. Estudo numérico dos meandros e vórtices da Corrente do Brasil entre 22°S e 30°S. Tese de doutorado. Pós-Graduação de Engenharia da Universidade Federal do Rio de Janeiro. Rio de Janeiro., 138p.

HAMILL TM 2006. Ensemble-based atmospheric data assimilation. Predictability of Weather and Climate, T. Palmer and R. Hagedorn, Eds., Cambridge University Press, 124–156.

HOFFMAN M, MIYOSHI T, HAINE T, IDE K, BROWN C, MURTUGUDDE R., 2012. An Advanced Data Assimilation System for the Chesapeake Bay: Performance Evaluation. Journal of Atmospheric and Oceanic Technology, 29(10):1542-1557.

HOUTEKAMER P, ZHANG F., 2016. Review of the Ensemble Kalman Filter for Atmospheric Data Assimilation. Monthly Weather Review, 144(12):4489-4532.

HURLBURT HE, BRASSINGTON G, DRILLET Y, KAMACHI M, BENKIRAN M, BOURDALLÉ-BADIE R, CHASSIGNET E, JACOBS G, GALLOUDEC O, LELLOUCHE J, METZGER E, OKE P, PUGH T, SCHILLER A, SMEDSTAD O, TRANCHANT B, TSUJINO H, USUI N, WALLCRAFT A., 2009. High-Resolution Global and Basin-Scale Ocean Analyses and Forecasts. Oceanography, 22(3):80-97.

HURLBURT HE, CHASSIGNET EP, CUMMINGS JA, KARA AB, METZGER EJ, SHRIVER JF, SMEDSTAD OM, WALLCRAFT AJ, BARRON CN., 2008. Eddy-Resolving Global Ocean Prediction. In Ocean Modeling in an Eddying Regime (eds M. W. Hecht and H. Hasumi), American Geophysical Union, Washington, D. C. 353-381.

KALNAY E., 2003. Atmospheric modeling, data assimilation and predictability. Cambridge [u.a.]: Cambridge University Press.

KALNAY E, KANAMITSU M, KISTLER R, COLLINS W, DEAVEN D, GANDIN L, IREDELL M, SAHA S, WHITE G, WOOLEN J, ZHU Y, CHELLIAH M, EBISUZAKI W, HIGGINS W, JANOWIAK J, MO KC, ROPELEWSKI C, WANG J, LEETMA A, REYNOLDS R, JENNE R, JOSEPH D., 1996. The NCEP/ NCAR 40-year reanalysis project, Bulletin of the American Meteorological Society, 77(3):437-471.

LEÃO EA., 2013. Investigação do Vórtice de Vitória: mecanismos responsáveis por sua geração, manutenção e propagação. Master's Dissertation in Postgraduate Program in Geophysics. Universidade Federal da Bahia, Fundação de Amparo à Pesquisa do Estado da Bahia. Portuguese., 113p.

LEITH CE., 1974. Theoretical skill of Monte Carlo forecasts. Mon. Wea. Rev., 102: 409-418.

LENTINI CAD, SOUZA RB., 2005. Eddies e vórtices de mesoescala no Oceano Atlântico Sudoeste medidos através de satélites. In: Oceanografia por satélites. Oficina de Textos, Barueri, SP, 166-178.

LIMA M, CIRANO M, MATA M, GOES M, GONI G, BARINGER M., 2016. An assessment of the Brazil Current baroclinic structure and variability near 22°S in Distinct Ocean Forecasting and Analysis Systems. Ocean Dynamics, 66(6-7):893-916.

LIMA J, MARTINS R, TANAJURA C, PAIVA A, CIRANO M, CAMPOS E, SOARES I, FRANÇA G, OBINO R, ALVARENGA J., 2013. Design and implementation of the oceanographic modeling and observation network (REMO) for operational oceanography and ocean forecasting. Revista Brasileira de Geofísica 31:209-228.

LORENZ EN., 1963. The predictability of hydrodynamic flow. Trans. NY Acad. Sci., Series II 25:409-432.

LORENZ EN., 1965. A study of the predictability of a 28-variable atmospheric model. Tellus 17: 321-333.

MANO M, PAIVA A, TORRES A, COUTINHO A., 2009. Energy Flux to a Cyclonic Eddy off Cabo Frio, Brazil. Journal of Physical Oceanography, 39(11):2999-3010.

MARTA-ALMEIDA M, RUIZ-VILLARREAL M, PEREIRA J, OTERO P, CIRANO M, ZHANG X, HETLAND R., 2013. Efficient tools for marine operational forecast and oil spill tracking. Marine Pollution Bulletin, 71(1-2):139-151.

MATA MM, CIRANO M, van CASPEL MR, FONTLESS CS, GOÑI G, BARINGER M., 2012. Observations of Brazil current baroclinic transport near 22°S: variability from the AX97 XBT transect. CLIVAR Exch 58(17):5– 10.

MCWILLIAMS JC., 2008. The Nature and Consequences of Oceanic Eddies. In: Ocean Modeling in an Eddying Regime (eds M. W. Hecht and H. Hasumi), American Geophysical Union, Washington, D. C. pp. 5-15.

MELSOM A, COUNILLION F, LACASCE J, BERTINO L., 2012. Forecasting search areas using ensemble ocean circulation modeling. Ocean Dynamics, 62(8):1245-1257.

MIGNAC D, TANAJURA C, SANTANA A, LIMA L, XIE J., 2015. Argo data assimilation into HYCOM with an EnOI method in the Atlantic Ocean. Ocean Science 11: 195-213.

MILL G, COSTA V, LIMA N, GABIOUX M, GUERRA L, PAIVA A., 2015. Northward migration of Cape São Tomé rings, Brazil. Continental Shelf Research, 106:27-37.

NEWTON TS., 2013. Estudo da ocorrência do Vórtice de Cabo Frio e do Vórtice do Cabo de São tomé. Tese de mestrado. Universidade de São Paulo, São Paulo, 77 p.

OKE P, BRASSINGTON G, GRIFFIN D, SCHILLER A., 2010. Ocean data assimilation: a case for ensemble optimal interpolation. Australian Meteorological and Oceanographic Journal, 59(1SP):67-76.

OKE P, SAKOV P, CORNEY S., 2007. Impacts of localisation in the EnKF and EnOI: experiments with a small model. Ocean Dynamics, 57(1):32-45.

OKE PR, SCHILLER A., 2007. Impact of ARGO, SST, and altimeter data on an eddy-resolving ocean reanalysis. Geophys Reasearch Lett. 34:L19601.

PEREIRA J, CIRANO M, MARTA-ALMEIDA M, AMORIM F., 2013. A regional study of the Brazilian shelf/slope circulation (13°-31°S) using climatological open boundaries. Revista Brasileira de Geofísica, 31(2):289-305.

PEREIRA J, GABIOUX M, MARTA-ALMEIDA M, CIRANO M, PAIVA A, AGUIAR A., 2014. The bifurcation of the western boundary current system of the South Atlantic Ocean. Revista Brasileira de Geofísica, 32(2):240-257.

SAHA S, MOORTHI S, WU X, WANG J, NADIGA S, TRIPP P, BEHRINGER D, HOU YT, CHUANG HY, IREDELL M, EK M. et al., 2014. The NCEP climate forecast system version 2. Journal of Climate, 27(6):2185-2208.

SAKOV P, COUNILLON F, BERTINO L, LISÆTER K, OKE P, KORABLEV A., 2012. TOPAZ4: an ocean-sea ice data assimilation system for the North Atlantic and Arctic. Ocean Science, 8(4):633-656.

SCHILLER A, BELL M, BRASSINGTON G, BRASSEUR P, BARCIELA R, De MEY P, DOMBROWSKY E, GEHLEN M, HERNANDEZ F, KOURAFALOU V et al., 2015. Synthesis of new scientific challenges for GODAE OceanView. Journal of Operational Oceanography 8: s259-s271.

SHU Y, ZHU J, WANG D, XIAO X., 2011. Assimilating remote sensing and in situ observations into a coastal model of northern South China Sea using ensemble Kalman filter. Continental Shelf Research, 31(6):S24-S36.

SIGNORINI SR, MIRANDA LB, EVANS DL, STEVENSON MR, INOSTROZA HMV., 1989. Corrente do Brasil: estrutura térmica entre 19° e 25°S e circulação geostrófica. Bolm Inst oceanogr., São Paulo, 37(1):33-49.

SILVEIRA ICA, LIMA J, SCHMIDT A, CECCOPIERI W, SARTORI A, FRANSCISCO C, FONTES R., 2008. Is the meander growth in the Brazil Current system off Southeast Brazil due to baroclinic instability? Dynamics of Atmospheres and Oceans, 45(3-4):187-207.

SILVEIRA ICA, SCHMIDT A, CAMPOS EJD, GODOI S, IKEDA Y., 2000. A corrente do Brasil ao largo da costa leste brasileira. Revista Brasileira de Oceanografia, 48(2):171-183.

SRINIVASAN A, CHASSIGNET E, BERTINO L, BRANKART J, BRASSEUR P, CHIN T, COUNILLON F, CUMMINGS J, MARIANO A, SMEDSTAD O, THACKER W., 2011. A comparison of sequential assimilation schemes for ocean prediction with the HYbrid Coordinate Ocean Model (HYCOM): Twin experiments with static forecast error covariances. Ocean Modelling, 37(3-4):85-111.

TALAGRAND O., 1997. Assimilation of observations, an introduction. J. Met. Soc. Japan Special Issue 75, 1B, 191-209.

TANAJURA C, SANTANA A, MIGNAC D, LIMA L, BELYAEV K, JI-PING X., 2014. The REMO Ocean Data Assimilation System into HYCOM (RODAS_H): General Description and Preliminary Results. Atmospheric and Oceanic Science Letters 7:464-470.

TURNER JP, WALKER JP, OKE PR., 2008. Ensemble member generation for sequential data assimilation. Remote Sensing of Environment 112, 1421–1433.

XIE J, COUNILLON F, ZHU J, BERTINO L., 2011. An eddy resolving tidal-driven model of the South China Sea assimilating along-track SLA data using the EnOI. Ocean Science, 7(5):609-627.

XIE J, ZHU J., 2010. Ensemble optimal interpolation schemes for assimilating Argo profiles into a hybrid coordinate ocean model. Ocean Modelling, 33(3-4):283-298.

YAN CX, ZHU J, XIE JP., 2010. An ocean reanalysis system for the joining area of Asia and Indian-Pacific Ocean, Atmos. Oceanic Sci. Lett., 3:81–86.

ZARON E., 2011. Introduction to Ocean Data Assimilation. In: Schiller A, Brassington GB, editors. Operational oceanography in the 21st century. Springer Science+Business Media B. V.; p.321-350.

APPENDIX A

The ensemble spreading for the HYCOM 1/12° domain is given in Figure 4. The temperature at 50 m and sea level anomaly standard deviation on the thirtieth day were calculated for all the members, only for MFORC and only for MIC. As expected, the largest SD values were given for the regions with higher variability: equatorial region, near the adjacent continental shelf and Brazil-Malvinas confluence area, located in the south of the HYCOM domain. The Brazil-Malvinas confluence area contains a strong SST front between warmer waters from BC, flowing to the south, and colder waters from the Malvinas Current, flowing to the north. Considering all the ensemble members, the highest temperature SD was 5.77°C, the mean temperature SD was 0.22°C. The largest SLA SD was 0.17 m and the mean SLA SD was 0.010 m. For MIC, the largest T SD was 6.84°C, the mean T SD was 0.33°C. The highest SD found for SLA was 0.16 m and the mean SLA SD was 0.006 m. For MFORC the largest T and SLA SD values were 5.69°C and 0.30 m, respectively, and the mean temperature and SLA SD found were 0.15°C and 0.018 m, respectively. The largest temperature SD was given for MIC due to the contribution of strategy 3, which perturbed the temperature with percentages of the SD added or subtracted to the control initial condition. Nonetheless, MFORC had greater contribution on the temperature SD in the Brazil-Malvinas confluence region than MIC members. The great temperature SD on the northeastern part of the HYCOM 1/12° domain was probably due to the high variability of the equatorial dynamic, like the great variability of the seasonal winds and the thermocline inclination. This reasserts the importance of these ensemble members on producing variability around the entire domain for SLA.

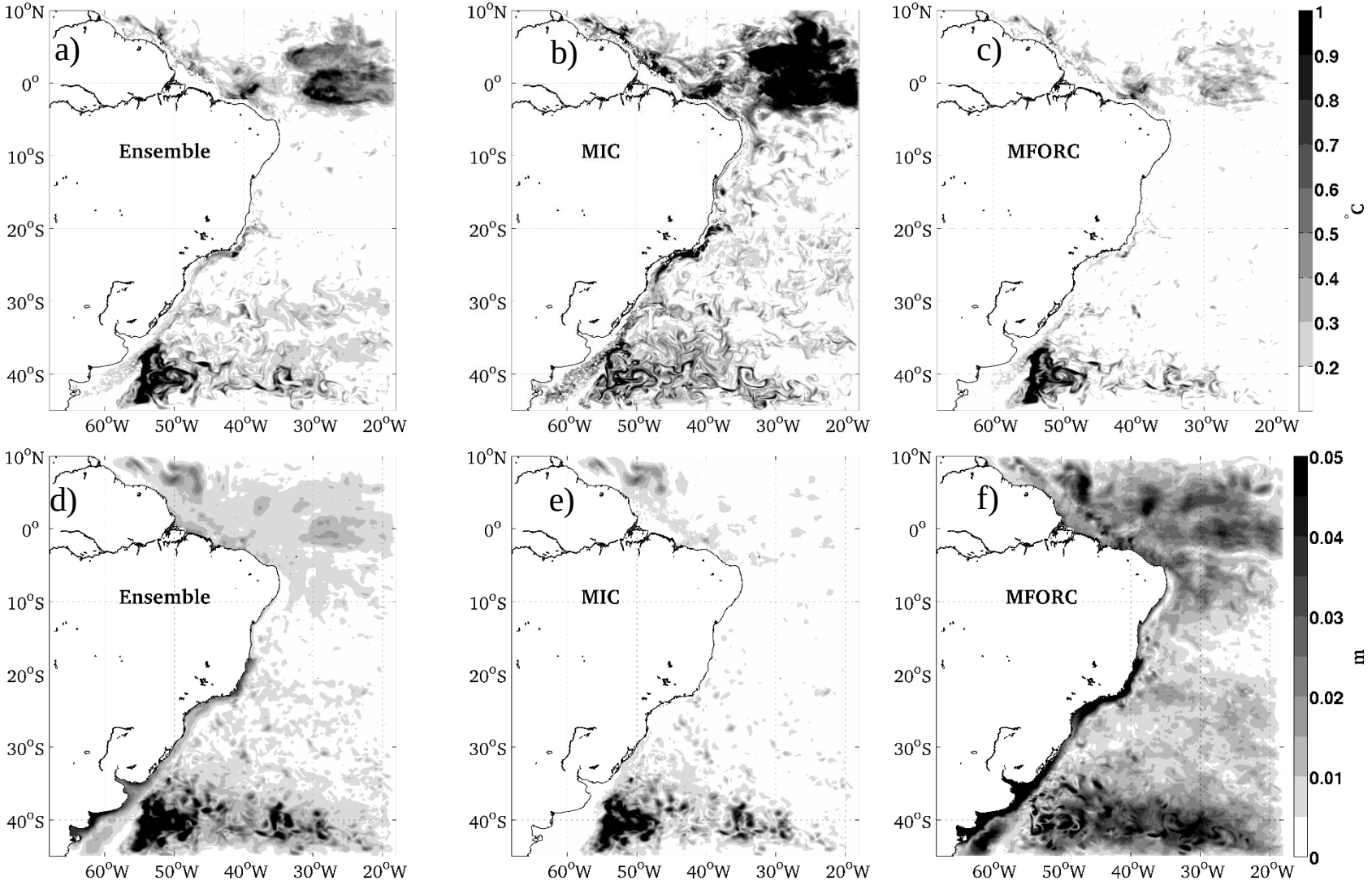

Figure A1. Temperature at 50m (upper panels) and sea level anomaly (bottom panels) standard deviation on day 30, among the ensemble members (a,d), only for the members with perturbed initial condition (MIC) (b,e) and only for the members with perturbed atmospheric forcing (MFORC) (c,f).